EFFECTS OF STRUCTURAL VISCOELASTICITY IN NON-DIVERGENCE FREE DEFORMABLE POROUS MEDIA WITH INCOMPRESSIBLE CONSTITUENTS

OGUNTOLA MICHEAL BABATUNDE

MASTER OF SCIENCE IN MATHEMATICS

(Computational Option)

PAN AFRICAN UNIVERSITY

INSTITUTE FOR BASIC SCIENCES,

TECHNOLOGY AND INNOVATION

2018

EFFECTS OF STRUCTURAL VISCOELASTICITY IN NON-DIVERGENCE FREE DEFORMABLE POROUS MEDIA WITH INCOMPRESSIBLE CONSTITUENTS

OGUNTOLA MICHEAL BABATUNDE

MC300-0004/17

A thesis submitted to Pan African University Institute for Basic Sciences, Technology and Innovation in partial fulfillment of the requirements for the award of the degree of Master of Science in Mathematics (Computational Option)

2018

DECLARATION

This thesis is my original work and it has not been submitted to any other university for a degree award.

Signature: _____ Date: _____

OGUNTOLA Micheal Babatunde

MC300-0004/17

This thesis has been submitted for examination with our approval as university Supervisors

Signature: _____ Date: _____

Professor Kinyanjui Mathew

Jomo Kenyatta University of Agriculture and Technology

Signature: _____ Date: _____

Professor Agure Ogonji John

Maseno University

DEDICATION

I dedicate this thesis to my parents Mr Tola Oguntola and Mrs Iyabo Oguntola, and my siblings for their kind love and support in terms of advice and prayers, to the love of my life Tanteliniaina Mioratina for her kindness and assistance, and to all my friends who have contributed positively through prayers and academic support during the course of this study.

Above all, I dedicate this thesis to the Almighty God who has, in His great and infinite mercy, given me the opportunity and strength to carry out this research.

ACKNOWLEDGMENT

Words cannot suffice to express my profound heart appreciation and gratitude to the Almighty God for giving me the unmerited grace for the successful preparation of this master's thesis, to Him be all the glory.

A special thanks to my supervisors, Prof. Kinyanjui Mathew and Prof. Ogonji John Agure for their exceptional guidance, monitoring and kind supports throughout the period of this master's thesis. I really appreciate your effort.

It is worthwhile to express my profound gratefulness to African Union Commission, and to all Pan African University, Institute for Basic Sciences, Technology and Innovations (PAUSITI) lecturers and staff for their support and encouragement.

From the bottom of my heart, I acknowledge the incomparable effort of my parents, Mr. and Mrs. T.I Oguntola, who gave me the legacy called formal education. Without them, I would be nowhere today. I also extend my heartfelt thanks to my siblings and friends for their emotional supports and constant communications. My sincere and awesome gratitude goes to my fiancée Tanteliniaina Mioratina for her unequal love, her devoted prayers, and enthusiastic assistance towards me.

Finally, to my colleagues, the third cohort students of Pan African University, Institute for Basic Sciences, Technology and Innovations (2016/2017 class), it was an awesomely wonderful time being with you all. I enjoyed every moment we shared together, the memories will forever linger in my heart. Wish you all success in your future endeavours. Thanks

TABLE OF CONTENTS

LIST OF FIGURES

LIST OF TABLES

NOMENCLATURES

Symbols	Meaning
α	Purely elastic effect of porous medium
β	Viscoelastic effect of porous medium
ΔV	Change in material volume (m^3)
δ	Viscoelastic effects for the solid components
$\epsilon(\vec{u})$	Volumetric strain
ϵ_0	Increment of fluid content at time $t = 0$
Γ_D	Boundary condition imposed on displacement
Γ_N	Boundary condition imposed on stress
λ_n	Eigenvalues (m^{-2})
$\mathbb{C}$	Set of complex numbers
$\mathbb{N}$	Set of natural numbers
$\mathbb{R}^n$	n-Dimensional Euclidean space
$\mathcal{C}$	Orthonormal sequence in H
$\mathcal{D}'(0, L)$	Space of distributions on $(0, L)$
$\mathcal{P}$	Fluid power density (Wm^{-3})
$\mathfrak{b}$	Biot Willi's constant
μ_e and λ_e	Lame elastic parameters

μ_v and λ_v	Viscoelastic parameters
∇u	Volumetric dialation
$\partial\Omega$	Boundary of the domain Ω
ϕ	Volumetric fraction of fluid component or porosity
ρ	Fluid mass density (Kgm^{-3})
σ	Effective stress in one dimension (Pa)
σ_e	Elastic stress contribution in one dimension (Pa)
σ_v	Viscoelastic stress contribution in one dimension(Pa)
τ_e	Characteristics elastic time constant
$\mathbf{E}(\vec{u})$	Infinitesimal strain tensor
$\mathbf{I}$	Identity tensor
$\mathbf{K}$	Permeability tensor (m^2)
$\mathbf{T}$	Effective stress (Pa)
$\mathbf{T}_e$	Elastic stress contribution (Pa)
$\mathbf{T}_v$	Viscoelastic stress contribution (Pa)
$\vec{B}$	Body force per unit of volume (Nm^{-3})
$\vec{t_{\vec{n}}}$	force per unit area (boundary traction)(Nm^{-2})
$\vec{u}$	Solid displacement (m)
$\vec{u}$	Solid displacement in $\mathbb{R}^n$ (m)
ζ	Variation of fluid content per unit volume of porous media (Nm^{-2})
$D^i v$	$i^{th}-$weak derivative of v.
F_{spec}	Magnitude of the boundary traction (Nm^{-2})

$H(t)$	Heavside function of t
K_0	Fixed medium permeability (m^2)
L	Length of material (m)
p	Darcy fluid pressure (Pa)
Q	Net volumetric fluid production rate $(m^3.s^{-1})$
s_ϵ	Storage cofficient of medium
T	Time (s)
u	Solid displacement (m)
u_0	Solid displacement at time $t = 0$ (m)
V	Material volume (m^3)
v	Discharge velocity (ms^{-1})
$V_f(\vec{x}, t)$	Volume occupied by the fluid constituents of porous medium (m^3)
$V_p(\vec{x}, t)$	Pore volume of the porous medium (m^3)
$V_s(\vec{x}, t)$	Volume occupied by the solid constituents of porous medium (m^3)
De	Deborah number

ABBREVIATIONS

PDEs . . . . . Partial differential equations

IBVP . . . . . Initial boundary value problem

NHLIBVP . . . . . Non-homogeneous linear initial boundary value problem

SVE . . . . . Structural viscoelasticity

DPMWIC . . . . . Deformable porous media with incompressible constituents

CCE . . . . . Confined compression experiments

ABSTRACT

In this thesis, the importance of structural viscoelasticity in the mechanical response of deformable porous media with incompressible constituents under sudden changes in the external applied quasi-static loads using mathematical analysis has been investigated. Here, the applied load is characterized by a step pulse or a trapezoidal pulse. Mathematical models of non-divergence free deformable porous media are often used to characterize the behaviour of biological tissues such as cartilages, engineered tissue scaffolds, and bones which are viscoelastic and incompressible in nature, and viscoelasticity may change with age, disease or by design. The problem is formulated as a mixed boundary value problem of the theory of poro-viscoelasticity, in which an explicit solution has been obtained using separation of variables technique coupled with Fourier series analysis in one-dimension. Further, dimensional analysis is utilized to identify dimensionless parameters that can aid the design of structural properties so as to ensure that the fluid velocity past the porous medium remains bounded below a given threshold to prevent potential damage. The study shows that the fluid mechanics within the medium can abruptly be altered if the applied load encounters a sudden change in time and structural viscoelasticity is too small. The analysis is used to explain the confined compression experiment clarifying the cause of micro-structural damages in biological tissues associated with loss of tissue viscoelastic property, which leads to the cause of diseases like Glaucoma.

CHAPTER 1

INTRODUCTION

1.1 Background of Study

Fluid flow in deformable porous media has many applications in biology, medicine, and bio-engineering. For examples, blood flow through tissues in the human body (Paola et al., 2014; Dominique et al., 2010; Khanafer et al., 2008; Yuan, 2014), and fluid flow through cartilages, bones and engineered tissue scaffolds which exhibit both elastic and viscoelastic behaviours resulting from the combined action of various components, such as elastin, collagen, and extracellular matrix (Recha-Sancho et al., 2016). From mathematical viewpoints, the study of fluid flow through deformable porous structures requires the coupling of poro-elasticity with structural viscoelasticity, leading to Poro-viscoelastic models. Interestingly, clinical evidence has shown that the loss of viscoelastic biological tissues properties which leads to their damages has been linked to various disease conditions such as atherosclerosis, Alzheimer's disease and glaucoma. This triggered the interests of scientists to investigate the cause of the micro-structural damages in the tissues.

Theoretical study of fluid flow through deformable porous media has attracted a lot of attention since the beginning of the last century. The development of the field started with the work of von Terzaghi (1925). But, it was Biot (1941) who set up the framework and ignited the mathematical development for fluid flow through poro-elastic media. Biot pioneered the development of an elastodynamics theory for a saturated elastic porous medium, which theory has had wide applications in the geophysics for analysing wave propagation characteristics under cyclic loads. To date, several books and articles have been devoted to the mathematical analysis and numerical investigation of poro-elastic models, such as Cao et al. (2013), with applications ranging from engineering and geophysics to medicine and biology. Lorena et al. (2016) devised

a theoretical and numerical framework to investigate poro-elastic and poro-viscoelastic models. The study showed that structural viscoelasticity plays an important role in determining the regularity requirements for volumetric and boundary forcing terms, as well as for the corresponding solutions of the models. More so, the solutions of fluid-solid mixture (elastic displacement, fluid pressure, and Darcy velocity) are more sensitive to the boundary traction in the elastic case than in the viscoelastic scenario (Banks et al., 2017).

The study by Lorena et al. (2016) has provided numerical clues that sudden changes in body forces and/ or stress boundary conditions may lead to uncontrollable fluid-dynamical responses within the medium in the absence of structural viscoelasticity. These theoretical findings are also supported by experimental and clinical evidence indicating that changes in tissue viscoelasticity are associated with various pathological conditions, such as atherosclerosis (Osidak et al., 2015), osteoporosis (Augat & Schorlemmer, 2006), renal disease (London et al., 2002) and glaucoma (Downs et al., 2005). Hence, sudden time variations in stress conditions coupled with lack of structural viscoelasticity in biological tissues could lead to microstructural damage due to local fluid-dynamical alterations (Verri et al., 2017).

This thesis has considered a non-linear system of partial differential equations that are often encountered when modeling fluid flow through deformable porous media. The non-linearity in the system is as a result of the medium permeability.

The relevance of the combination between structural mechanics and fluid dynamics in the damage of deformable porous media has been the focus of many authors (Nia et al., 2011; Selvadurai, 2003). This thesis investigated a particular aspect of this combination and focused on characterising and quantifying the role of structural viscoelasticity on the biomechanical response to abrupt changes in stress conditions.

1.2 Definition of terms

This section presents definitions of terms which are fundamental to the entire work and also consider preliminaries which play a crucial role in the present study.

1.2.1 Viscoelasticity

This is a material behaviour which is a blend of both elastic and viscous properties (Shabana, 2018). Viscoelastic materials are materials that exhibit the following behaviours:

(i) Creep: This is a continued deformation over time of a body maintained under a constant stress. Example: Creep indentation of articular cartilage

(ii) Stress relaxation: This is when a body is suddenly strained and the strain is maintained, while the stress in the body decreases over time. Example: Stress relaxation of a soft tissue, e.g., tendon, ligament, skin under tension.

(iii) Hysteresis: This is the dissipation of energy during loading–unloading cycles. Example: Cyclic tensile loading of articular cartilage, knee meniscus, or temporomandibular joint disc.

(iv) Strain-rate-dependent properties: This is when the stress–strain behavior of a material depends on the strain rate (Athanasiou & Natoli, 2008).

1.2.2 Porous medium

This is a solid containing an interconnected network of pores (voids) filled with a fluid (liquid or gas). The solid matrix and the pore fluid are assumed continuous, forming two inter-penetrating continua (example, biological tissues) (Athanasiou & Natoli, 2008). A porous solid made of a solid matrix and of a connected pore space saturated by a fluid mixture is called a fluid–solid mixture. It can be viewed as a deformable open system exchanging fluid mass with the surroundings when subjected to loading and unloading (Coussy, 2004). The porosity relative to a volume of porous solid is the fraction of that volume formed from pores (Coussy, 2004).

The Storage coefficient of a porous medium is the volume of fluid stored into or extracted from a unit volume of the medium per unit increase or decrease in fluid pressure. It quantifies the storage capacity of a porous medium (Cheng, 2016). Fluid content increment is defined as the amount of fluid volume entering the porous medium per unit volume of the medium.

Definition 1.2.1. Poromechanics is the study of porous materials whose mechanical behaviour is significantly influenced by the pore fluid (Coussy, 2004).

Definition 1.2.2. Poro-elasticity is the study of elastic deformation of porous materials saturated with a fluid and the coupling between the fluid pressure and the solid deformation (Lu & Mow, 2008).

Definition 1.2.3. Poro-viscoelasticity is the study of the coupling of structural viscoelasticity with theory of poro-elasticity.

Definition 1.2.4. Volumetric strain or dilatation is the change in volume per unit volume of the medium.

1.2.3 Darcy's law

This is a constitutive equation that describes the flow of fluid through a porous medium (Athanasiou & Natoli, 2008). The Darcy velocity or the filtration velocity, is the superficial velocity that would occur if the entire cross section of the porous solid, and not just the pores, would be open to flow. It can also be interpreted as a volumetric flux (Jansen, 2013).

1.2.4 Confined compression

Tis is an idealized deformation configuration in which a porous material (tissue specimen) is placed into a chamber that confines the specimen at the bottom and on the sides. A porous platen called permeable piston , which allows fluid to exit through the specimen's surface, is used to compress the sample (Athanasiou & Natoli, 2008).

1.3 Statement of the problem

Theories of poro-elasticity have been developed and used extensively to model fluid flow through porous media in engineering and fluid flow in biological tissues (Čanić et al., 2006; Holzapfel & Ogden, 2017). It was found that most of these theories give no account for the role of structural viscoelasticity in the medium mechanical response when subjected to a loading system and hence conditions leading to abrupt alteration in the fluid mechanics within the porous medium have not been investigated extensively on this account.

This thesis utilized mathematical analysis coupled with the theory of poro-viscoelasticity to investigate the effect of structural viscoelasticity on the mechanical response of non-divergence free deformable porous medium with incompressible constituents when subjected to quasi-static load and hence provided conditions leading to abrupt fluid mechanics alteration within the porous medium. Experimentally, it has been shown in the literature that changes in biological tissue viscoelasticity are associated with various pathological states, such as Atherosclerosis, Glaucoma (Osidak et al., 2015; Maccabi et al., 2018). Therefore the need for this study.

1.4 Justification of Study

Problems involving deformation of porous media such as soft biological tissues are among the most challenging in applied mechanics. In addition to undergoing large strains, these media exhibit non-linear time-dependent behaviour similar to that of viscoelastic materials. As the first approximation, nonlinear elasticity theory was employed to investigate the mechanics of soft tissues, and thus severely restricting the range of biomechanics applications. However, extending the study to investigate the mechanics of poro-viscoelastic materials, open the way for a wider range of applications in tissue-engineering, geophysics, and biomechanics. The study of the role of viscoelasticity in deformable porous media is of immense importance and serves a wide variety of practical applications in processes such as consolidation, confined and unconfined compression test in biomechanics, experimental design of bioengineering tissue, polymeric foams involved in packing applications. Experimentally, it has been shown that loss of structural viscoelasticity contributes to the cause of illness like glaucoma(Osidak et al., 2015). Therefore, the reason for the present study is to provide theoretical and numerical evidence for the experimental results confirming structural viscoelasticity as the key determining factor of the fluid-velocity blow-up in biological tissues (like cartilages), a deformable porous medium with incompressible constituents, which leads to their damages. Also, the present study is an extension of the work in (Oguntola et al., 2018).

1.5 Objective of the Study

1.5.1 General objective

The main objective of this work is to investigate the effect of structural viscoelasticity in non-divergence free deformable porous media with incompressible constituents when subjected to Quasi-static mechanical loading and unloading system.

1.5.2 Specific objectives

The specific objectives of this study are:

i) To construct mathematical model of deformable one-dimensional poro-viscoelastic medium with incompressible constituents.

ii) To determine a unique weak solution of model in which the external applied load is characterized by a step pulse or a trapezoidal pulse in time

iii) To determine the effect of varying viscoelasticity on the fluid-dynamics in the porous medium

iv) To apply the mathematical analysis constructed to study some important features of confined compression creep experiment in biomechanics.

1.6 Significance of Study

The mathematical analysis provided in this research is very significant considering the importance of structural viscoelasticity in biomechanics as a whole and particularly can be utilized to study some interesting features of confined compression tests, which are often used in petroleum engineering, tissue engineering, and biomechanics respectively to characterize the mechanical and structural behaviour of porous media (example biological tissues). More so, the results of the present study provide series of conditions leading to the cause of the fluid-velocity blow-up and hence the blow-up of the fluid power density that was hypothesized by the theoretical

work presented in (Lorena et al., 2016), and consequent micro-structural soft biological tissues damages.

In Africa, issues related to borehole stability like pipe explosion etc. could be solved should proper designs of structural properties such as viscoeslaticity as presented in this study be followed. Also, micro-structural damages of biological tissues in Tissue Engineering can be solved by the present study.

1.7 Scope of the Study

The study is limited to the mathematical analysis of the effect of SVE in a deformable porous medium whose components are incompressible, under mechanical loading. Moreover, we consider a case where the strain in the porous medium under mechanical loads is infinitesimal. In particular, the cases where the medium is modeled as a poro-viscoelastic fluid-solid mixture, and the mechanical loads are characterised by step and trapezoidal pulses in one dimension is considered. The next chapter documents literature that are of great importance to the present study.

CHAPTER 2

LITERATURE REVIEW

Many porous media of interest in biomechanics including synthetic polymer, almost all biological materials (cells and tissues), and metals at high-temperature exhibit gradual deformation and recovery when subjected to loading and unloading system. The mechanical response of such materials depends upon how quickly the load is applied or removed, and the extent of deformation relies on the rate at which the external loads are applied. This time-dependent material behaviour is called the structural viscoelasticity.

Cao et al. (2015) and Kim (2017) investigated the flow of viscoelastic fluids through porous media and concluded that the analysis of flow in converging channels suggests that the pressure drop should increase to values well above those expected for purely viscous fluids at Deborah number levels of the order of 0.1 to 1.0. Their experimental results using a porous medium support this analysis and yield a critical value of the Deborah number of about 0.05 at which viscoelastic effects were first found to be measurable. Following the fact that viscoelastic effect could be measured. De et al. (2017) investigated the flow of unsteady 3D viscoelastic fluid through the array of symmetric and asymmetric sets of cylinders forming a model porous medium. A finitely extensible nonlinear elastic constitutive model with peterlin closure was used to model the viscoelastic part. The solid-fluid interfaces of the porous structures followed a second-order immersed boundary method (De et al., 2016), and the simulations therein gave insight into how flow structures, viscoelastic stresses, and viscoelastic work change with increasing Deborah number De.

Although, measuring the viscoelastic behaviour of highly hydrated biological materials has been a major challenge because of their intrinsic softness and labile nature. Tirella et al. (2014) formulated a method (elpsilon dot method) for deriving the viscoelastic parameters of soft hydrated biomaterials which can be used to rapidly test degradable samples. This method was

used to investigate the viscoelastic behaviour of porcine liver and the results showed that the constitutive parameters of hepatic tissue can be quickly quantified without the application of any prestress and before the onset of time-dependent degradation phenomena.

The biphasic theory is a simplification of mixture theory, where there are only two phases or constituents. In general, mixture theory describes a material as a continuum mixture of n phases, such that each spatial point in the mixture is occupied simultaneously by all the phases (Siddique et al., 2017). The first biphasic theory involved the modeling of biological tissues as a mixture of two distinct phases: an incompressible, porous solid phase to describe the collagen-proteoglycan matrix and an incompressible fluid phase to represent the interstitial fluid (Moore et al., 2015). The constitutive equations, continuity equations, and momentum equations were derived. This theory was applied to study biphasic creep and biphasic stress relaxation (Holzapfel & Ogden, 2017). Further, the Galerkin weighted residual method was applied to the momentum equation, and mechanical boundary conditions of both solid phase and the liquid phase. The penalty method was employed to deal with the intrinsically incompressible binary mixture problem. The solid phase displacement $(u)-$fluid phase velocity (v) form was adopted to express the weak form of the weighted residual statements for the solid and fluid phases (Yang, 2006). It was demonstrated that the viscoelastic behavior of the tissue is not only due to the diffusive interaction between the solid matrix and the interstitial fluid (flow-dependent), but also to the intrinsic viscoelasticity of the solid (flow-independent), and therefore many models were developed to describe it.

Triphasic theory considers a deformable porous medium like soft biological tissue as a mixture of three phase: an incompressible solid phase, an incompressible fluid phase and an ion phase of two types (cations and anions) of a single salt (Lai et al., 1991; Lu & Mow, 2008). This theory is the combination of the physical-chemical theory for ionic and polyionic solutions with the biphasic theory for cartilage. The momentum equations include chemical potentials whose gradients are the driving forces for movements of ions. The chemical potentials are determined by fluid pressure, salt concentration, solid matrix dialation, and fixed charge density. The triphasic theory was extended to model the mechano-electrochemical behaviors of charged - hydrated soft tissues which contain multi-electrolytes (Serpieri & Travascio, 2017). There are n+2 phases such as 1 charged solid phase, 1 non charged solvent phase and n ion species. The

corresponding continuity equations, momentum equations, and constitutive equations were derived, and the finite element method for the extended theory was formulated. Similarly, the chemo-electro-mechanical formulation of quasi-static finite deformation of swelling incompressible porous media was derived from mixture theory, in which four phases are defined: solid, fluid, anions and cations (Loret & Huyghe, 2014). Using the assumption of incompressible and isothermal deformation, balance laws are derived for each phase and for the mixture as a whole. This model was applied to study the intervertebral disc tissue (Jacobs et al., 2014).

The concept of porous medium flow originally emanated in soil mechanics, and more specifically in the works of (Von Terzaghi, 1923), in which a model was first developed for the creep phenomenon of saturated clay as a soil consolidation process. it was found that when a uniform surcharge is suddenly applied to the top of a clay layer, the soil is initially undrained and an initial excess pore pressure is generated which dissipates through the top surface. The dissipation follows a one-dimensional diffusion equation (Coussy, 2004). (Rendulic, 1936) extended the work by Tarzaghi to a three-dimensional form for the purpose of multi-dimensional consolidation problems.

The development of the theory of dynamic poro-elasticity gives a complete and general description of the mechanical behaviour of a poro-elastic medium (Athanasiou & Natoli, 2008; Coussy, 2004). The theory utilized the equations of linear elasticity for the solid matrix, Navierstokes equation for viscous fluid and Darcy's law for the flow of fluid through the porous matrix to derive the theory of linear poro-elasticity. In this work, it was shown that the one-dimensional diffusion equation is not satisfied by the pore pressure but by the relative volumetric strain between the porous medium frame and the fluid (Coussy, 2004).

In field applications, one of the challenging problems often encountered is borehole stability. Drilling difficulties are associated mainly with tufaceous sediments and shales, and typical problems encountered in shales are drill-tool sticking, sloughing, and creep in the borehole wall. The cause of these problems can be of chemical and/or mechanical nature. But, even in oil-based mud, which is free from chemical effects still suffers borehole instability remains. Part of the difficulties can be attributed to the mechanical effects of poro-elastic and viscoelastic origins (Coussy, 2004). In this regard was the theory of poro-viscoelasticity developed.

Simon et al. (1985) considered the soft tissues in the spinal motion segment as poro-elastic

structures which were treated as a fluid phase flowing through the pores of a deformable porous solid skeleton or solid phase. A displacement of solid phase $(u)-$displacement of fluid phase (w) formulation was utilized where the fluid motion is relative to the deforming solid phase under mechanical loading. The field equations by Biot (1941) include an overall dynamic equilibrium equation and a generalized Darcy law for the dynamic equilibrium for the fluid motion. After, Simon et al. (1985) extended this work to large strains and derived the Lagrangian forms of the governing equations (Holzapfel & Ogden, 2017).

Soltz & Ateshian (1998) showed that biological tissues interstitial fluid pressurization supports the majority of the applied load, in the testing configurations of confined compression creep and stress relaxation.

Research has shown that the mechanical properties of biological tissues differ significantly from those of rocks. Specifically, since most of the biological tissues are composed by both elastin and collagen, the deformable matrix within the porous medium exhibits both elastic and viscoelastic behaviors. More so, material properties and volume fractions of elastic and collagen vary in health and disease, thereby motivating a detailed investigation of their influence on the physical system and, consequently, on the solution of the PDEs describing this system. Lorena et al. (2016) considered a physical system which described the motion of fluid-solid mixture under the assumption of full saturation, whereby the ability of the fluid phase to flow within the solid skeleton is described by the permeability tensor, which is assumed to be a multiple of the identity tensor and to depend nonlinearly on the volumetric solid strain. Therein, the problem of the existence of weak solutions in bounded domains, accounting for non-zero volumetric and boundary forcing terms was studied, and the influence of viscoelasticity was investigated on the solution functional setting and on the regularity requirements for the forcing terms. Under the assumptions of small deformation, full saturation of solid-fluid mixture, incompressible mixture constituents and negligible inertia Lorena et al. (2016) formulated a nonlinear system of PDEs to model fluid flow through deformable porous media (solid-fluid mixture) and the requirements (like elliptic regularity) for existence of solution for the case when $\delta = 0$ were investigated. Following the analytic solutions provided by Lorena et al. (2016) and Verri et al. (2017) for poro-viscoelastic models inspired by problems in medicine and biology, Banks et al. (2017) performed sensitivity analysis on the solutions of these fluid-solid mixtures problems

with respect to the imposed boundary data, which are the main drivers of the system for optimization purposes.

The prescribed assumptions by Lorena et al. (2016), followed by Verri et al. (2017) makes it possible to formulate a concept to study the effect of viscoelasticity on deformable porous media with incompressible constituents, that's in some sense close to reality, as verified by experimental and clinical facts, even though the situation of "negligible inertia" is not visible, in addition to assuming that the media constituents are incompressible and isotropic.

Furthermore, in the one-dimensional poro-viscoelastic model considered by Verri et al. (2017), the prescribed multiplicative term for the stress due to the viscoelastic effect to indicate the extent to which the model includes the viscoelasticity effect of the solid components was not utilized. Also, the nature of the medium and the type of loading and unloading system considered for the model constructed in Verri et al. (2017) wasn't pointed out. In application, the importance of the coupling of structural viscoelasticity with poro-elasticity in biomechanics, petroleum engineering, and tissue engineering cannot be overemphasized, but most of the theoretical studies focused on the poro-elastic case without accounting for structural viscoelasticity. Therefore, this study intends to investigate the effects of structural viscoelasticity in the mechanical response of non-divergence free deformable porous medium under a quasi-static loading system using mathematical analysis and then utilizes the construction to explain some important features of the confined compression experiment in biomechanics.

The next chapter provides the methodology and governing equations that are utilized in the present study.

CHAPTER 3

METHODOLOGY AND GOVERNING EQUATIONS

3.1 Introduction

This chapter utilizes the theory of poro-viscoelasticity presented in Verri et al. (2017) and (Lorena et al., 2016) to construct a one-dimensional model involving the coupling of structural viscoelasticity and poro-elasticity to describe the motion of a non-divergence free deformable of porous medium with incompressible constituent under the influence of quasi-static loading conditions. In contrast to the theory of elasticity, the non-divergence free porous medium here is to mean that the incompressibility of each component of the medium doesn't mean that both solid displacement and fluid velocity are divergence-free. This follows from the fact that the medium undergoes deformation (infinitesimal) under the applied external load (Athanasiou & Natoli, 2008; Lai et al., 2009). The quasi-static loading condition is to mean negligible inertia. In this regard, the external loads are characterised by step and trapezoidal pulses in time.

Separation of variables technique with the theory of Fourier series is used to obtain an explicit solution for the solid displacement. The well-posedness of the solution is shown using some properties of a special type of Sobolev space, and then the fluid discharge velocity and power density in the porous medium are discussed.

Furthermore, dimensional analysis is utilized to formulate the dimensionless form of the one-dimensional poro-viscoelastic equations for the purpose of identifying parameters that most influence the solutions' properties and hence providing the direction for sensitivity analysis on the system which can help in the experimental design in Tissue engineering.

3.2 General Poro-viscoelastic Model Formulation and Description

Consider a deformable porous medium as a continuum and let $\Omega \subset \mathbb{R}^n,\ n = 1, 2, 3$ be a bounded open and connected domain with a lipschitz continuous boundary $\partial\Omega$, and a unit outward normal , $\hat{n}$ occupied by the medium (fluid-solid mixture). Let

$$\vec{u} : \Omega \times (0, T) \longrightarrow \mathbb{R}^n$$

be the displacement of the porous medium, and $\mathbf{E}(\vec{u})$ be the infinitesimal strain tensor for each time $t \in (0, T)$ with $0 < T < \infty$.

3.2.1 Assumptions

This study assumes that there is

iv) Quasi-static loading (negligible inertia),

i) Infinitesimal(very small) deformation,

ii) Full saturation in the porous medium, and

iii) Incompressible porous medium's constituents

and then the motion and the mechanical response of the deformable porous medium under quasi-static loading are described by two set of equations, namely the balanced and constitutive equations.

3.3 Balance equations

These involve the balance of mass equation for the fluid content in the medium and the balance of linear momentum for the fluid-solid mixture of the medium. Here, the set of balance equations often encountered in modeling fluid flow through porous media are considered. Let $V_s(\vec{x}, t)$ and $V_f(\vec{x}, t)$ be the volumes occupied by the solid and fluid constituents at

$(\vec{x}, t) \in \Omega \times (0, T)$ respectively. In every volume $V(\vec{x}, t)$ of a porous medium centered at $\vec{x} \in \Omega$ at time t, the volumetric fraction, $\phi(\vec{x}, t)$ of the fluid constituents given by

$$\phi(x, t) = \frac{V_f(\vec{x}, t)}{V(\vec{x}, t)}. \tag{3.3.1}$$

is called the Porosity of the medium (Lorena et al., 2016). If $V_p(\vec{x}, t)$ is the pore volume of the medium, under full saturation condition, we have

$$V_p(\vec{x}, t) = V_f(\vec{x}, t),$$

and the volumetric fraction of the solid component of the medium is given by:

$$1 - \phi(\vec{x}, t). \tag{3.3.2}$$

The motion of the poro-viscoelastic material is governed by the following balance of mass equation for the fluid component:

$$\frac{\partial \zeta}{\partial t} + \nabla \cdot \vec{v} = Q(x, t) \qquad \text{in } \Omega \times (0, T) \tag{3.3.3}$$

where, $\vec{v}$ is the discharge velocity, Q is the net volumetric fluid production rate (source term for fluid mass), The balance of linear momentum equation for the fluid-solid mixture under quasi-static loading is:

$$\nabla \cdot \mathbf{T} + \vec{B} = 0 \qquad \text{in } \Omega \times (0, T). \tag{3.3.4}$$

where, $\mathbf{T}$ is the stress tensor of the mixture (also called total stress), $\vec{B}$ is the body force per unit volume (source term of linear momentum).

In continuum mechanics, the source terms Q and $\vec{B}$ are defined respectively by

$$Q = \phi Q_f, \text{ and } \vec{B} = \rho f - \rho_f Q_f v - \rho_f \phi Q_f \frac{\partial \vec{u}}{\partial t}, \tag{3.3.5}$$

where $\rho = \rho_f\phi + \rho_s(1-\phi)$ is the mixture density, ρ_f and ρ_s are the specific densities of the fluid and solid components, $\vec{u}$ is the solid displacements, and Q_f and f are given data (Lorena et al., 2016).

Biomechanical applications are characterised based on tissues having the same mass density as water and as such, this research considered the situation whereby deformable porous media are composed of incompressible solid and fluid components. It follows from Biot's theory of poroelasticity (in $\mathbb{R}^n,\ \ n = 1, 2, 3$) that increment of fluid content ζ is given by;

$$\zeta = \mathfrak{b}\epsilon(\vec{u}) + s_\epsilon p, \tag{3.3.6}$$

where $\mathfrak{b}$ is the Biot Willi's constant, $\vec{u}$ is the solid displacement, $\epsilon(\vec{u})$ is the volumetric strain, s_ϵ is storage coefficient of medium and p is the fluid pressure. For incompressible constituents of porous medium, $\mathfrak{b} = 1,\ \ s_\epsilon = 0$ (Coussy, 2004). Thus (3.3.6) reduces to

$$\zeta = \epsilon(\vec{u}). \tag{3.3.7}$$

The volumetric strain $\epsilon(\vec{u}) = \frac{\Delta V}{V}$ is known as Dilatation which is given by:

$$\epsilon(\vec{u}) = \nabla \cdot \vec{u},$$

and as such, the fluid content increment in (3.3.7) becomes

$$\zeta = \nabla \cdot \vec{u}, \tag{3.3.8}$$

and the volumetric strain of solid constituents lead to the variations of the fluid content of the porous medium. Use the convention $\nabla \cdot \vec{u}$ positive to mean extension implying "gain" of fluid in the medium (Wang, 2017).

3.3.1 Constitutive equations

These include equations that quantify the total stress, discharge velocity and fluid contents respectively. For the purpose of our analysis, we consider the following constitutive equations

$$\left.\begin{aligned} \mathbf{T} &= \mathbf{T}_e + \delta\mathbf{T}_v - p\mathbf{I} \\ \mathbf{T}_e &= \lambda_e(\nabla\cdot\vec{u})\mathbf{I} + 2\mu_e\mathbf{E}(\vec{u}) \\ \mathbf{T}_v &= \lambda_v(\nabla\cdot\frac{\partial\vec{u}}{\partial t})\mathbf{I} + 2\mu_v\mathbf{E}(\frac{\partial\vec{u}}{\partial t}) \\ \zeta &= \nabla\cdot\vec{u} \\ \vec{v} &= -\mathbf{K}\nabla p, \end{aligned}\right\} \tag{3.3.9}$$

where p is the Darcy fluid pressure, $\mathbf{I}$ is the identity tensor, $\mathbf{E}(\vec{u})$ is the infinitesimal strain tensor. Also

$$\mathbf{E}(\vec{u}) = \frac{\nabla\vec{u} + (\nabla\vec{u})^T}{2}. \tag{3.3.10}$$

$\mathbf{E}(\vec{u})$ is the same as the symmetric part of the gradient of the displacement vector field $\vec{u}$. λ_e, and μ_e are the Lame elastic parameters, λ_v and μ_v are viscoelastic parameters. $\mathbf{T}_e$, and $\mathbf{T}_v$ are the elastic and viscoelastic stress contributions respectively. The parameter $\delta \geq 0$ indicates the extent to which the model includes viscoelastic effect for the solid component, with $\delta = 0$, corresponds to the purely elastic case. The system of equations (3.3.3) to (3.3.9), with $\delta > 0$ characterises the motion of a poro-viscoelastic medium under quasi-static loading in $\mathbb{R}^n$, $n = 1, 2, 3$. Further, the parameter $\mathbf{K}$ is the porous medium permeability tensor which may depend on space and dilation, that's

$$\mathbf{K} = \mathbf{K}(x, \nabla\cdot\vec{u})$$

(Jeanne et al., 2018) and (Ghabezloo et al., 2009). In addition to the system of PDEs (3.3.3) to (3.3.9), the following Dirichlet-Neumann boundary and initial conditions are considered:

3.3.2 Boundary conditions

Suppose that the boundary $\partial\Omega$ of Ω can be decomposed as

$$\partial\Omega = \Gamma_N \cup \Gamma_D \text{ with } \Gamma_D = \Gamma_{D,p} \cup \Gamma_{D,v}$$

and possibly

$$\Gamma_D \cap \Gamma_v = \emptyset$$

then

$$\left.\begin{aligned} \mathbf{T}\vec{n} = \vec{t}_{\vec{n}}, \;\; \vec{v}\cdot\vec{n} = 0 \quad & \text{on } \Gamma_N \times (0,T) \\ \vec{u} = \vec{0}, \;\; p = 0 \quad & \text{on } \Gamma_{D,p} \times (0,T) \\ \vec{u} = \vec{0}, \;\; \vec{v}\cdot\vec{n} = \psi \quad & \text{on } \Gamma_{D,v} \times (0,T) \end{aligned}\right\} \tag{3.3.11}$$

Here the subscripts N and D indicates boundary conditions imposed on stress and displacement, whereas the subscripts p and v indicate conditions imposed on Darcy pressure and velocity, $\vec{t}_{\vec{n}}$ is the force per unit area (surface traction), and ψ is a prescribed function of space and time.

3.3.3 Initial conditions

For the initial conditions, it is important to differentiate between two cases, namely viscoelastic case ($\delta > 0$) and purely elastic case ($\delta = 0$).

When $\delta > 0$, the equations of balance of mass and linear momentum contain time derivatives, thus requiring an initial conditions on the whole displacement field $\vec{u}$. That's

$$\vec{u} = u_0 \quad \text{at } \; t = 0 \;\; \text{ in } \; \Omega \tag{3.3.12}$$

and when $\delta = 0$, only the increment in fluid content in the mass balance equation undergoes time derivative, and as such we have

$$\nabla \cdot \vec{u} = \epsilon_0 \quad \text{at } \; t = 0 \;\; \text{ in } \; \Omega, \tag{3.3.13}$$

where u_0, and ϵ_0 are prescribed initial data. Therefore equations (3.3.3) to (3.3.13) are known as an Initial Boundary Value Problem (IBVP) and the requirements (like elliptic regularity) for existence of solution for the case when $\delta = 0$ has been investigated in Lorena et al. (2016). For constant medium permeability, the resulting coupling between elastic equations and fluid subproblem is linear and the existence, uniqueness and regularity of solutions have been studied

by many authors (Owczarek, 2010; Showalter, 2000).

The following section presents a one-dimensional poro-viscoelastic model, for which an explicit solution is obtained and study the effect of structural viscoelasticity on the poro-mechanical response of the deformable porous medium to sudden changes in time-dependent mechanical load.

3.4 One-dimensional poro-viscoelastic problem formulation

Let the domain Ω be given as the open and bounded interval $(0, L) \subset \mathbb{R}$, with $0 < L < \infty$ and assuming in addition that there is no chemical reactions and no body force per unit volume, then $Q = \vec{B} = 0$ (Hutter et al., 2016; Verri et al., 2017). Let $\sigma,\ \sigma_e,\ \sigma_v,\ u,\ v$ and K be the one-dimensional form of $\mathbf{T},\ \mathbf{T}_e,\ \mathbf{T}_v,\ \vec{u},\ \vec{v}$ and $\mathbf{K}$ respectively. In this case, the increment of fluid content in (3.3.8) yields $\zeta = \frac{\partial u}{\partial x}$, so that the balance of mass equation in (3.3.3) becomes

$$\frac{\partial^2 u}{\partial t \partial x} + \frac{\partial v}{\partial x} = 0 \qquad \text{in } (0, L) \times (0, T). \tag{3.4.1}$$

The linear momentum equation in (3.3.4) gives

$$\frac{\partial \sigma}{\partial x} = 0 \qquad \text{in } (0, L) \times (0, T), \tag{3.4.2}$$

and the constitutive equations in (3.3.9) yields

$$\sigma = \sigma_e + \delta\sigma_v - p \tag{3.4.3}$$

where,

$$\begin{aligned} \sigma_e &= \lambda_e(\frac{\partial u}{\partial x}) + 2\mu_e \frac{\partial u}{\partial x} \\ &= \alpha \frac{\partial u}{\partial x}, \qquad (\text{where } \alpha = \lambda_e + 2\mu_e) \end{aligned} \tag{3.4.4}$$

$$\begin{aligned} \delta\sigma_v &= \delta\left(\lambda_v(\frac{\partial^2 u}{\partial x \partial t}) + 2\mu_v(\frac{\partial^2 u}{\partial x \partial t})\right) \\ &= \beta(\frac{\partial^2 u}{\partial x \partial t}), \qquad (\text{where } \beta = \delta(\lambda_v + 2\mu_v)) \end{aligned} \tag{3.4.5}$$

and

$$v = -K\frac{\partial p}{\partial x}, \tag{3.4.6}$$

in $(0, L) \times (0, T)$ respectively where we suppose that $0 \leq \delta \leq 1$, α indicates purely elastic effect, and β indicates viscoelastic effect in the medium.

Substituting (3.4.3), (3.4.4), and (3.4.5) into (3.4.2) gives

$$\alpha\frac{\partial^2 u}{\partial x^2} + \beta\frac{\partial^3 u}{\partial x^2 \partial t} - \frac{\partial p}{\partial x} = 0 \qquad \text{in } (0, L) \times (0, T). \tag{3.4.7}$$

Now suppose that the deformable porous medium with incompressible constituents under boundary traction (forcing term) $F(t)$, is as shown in Fig (3.1). Here, the forcing term $F(t)$ may have discontinuities in time, and the deformable porous medium may be either poro-elastic or poro-viscoelastic.

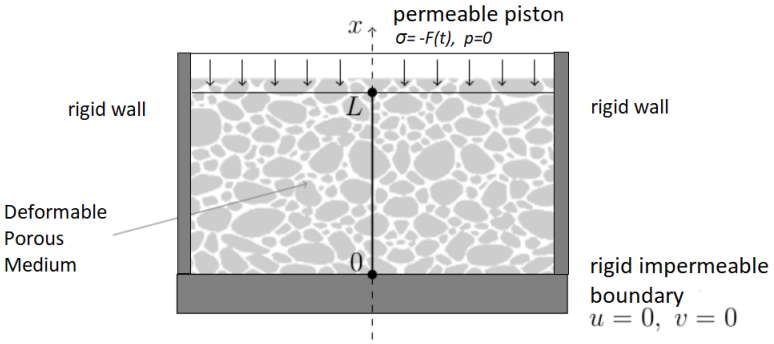

Figure 3.1. Schematic representation of the one-dimensional problem.

Then applying to the system of PDEs in (3.4.1) to (3.4.7), the following set of boundary and initial conditions which follows from (3.3.11)

$$u(0, t) = v(0, t) = 0 \qquad \forall\, 0 < t < T \tag{3.4.8}$$

$$p(L, t) = 0; \quad \sigma(L, t) = -F(t) \qquad \forall\, 0 < t < T \tag{3.4.9}$$

$$u(x, 0) = 0 \qquad \forall\, 0 < x < L \tag{3.4.10}$$

where $F(t)$ is the boundary forcing term (traction force).

If $\beta = 0$ (absent of viscoelasticity) in (3.4.5), with the medium permeability K, and the boundary forcing term $F(t)$ are given constants, then the system (3.4.1) to (3.4.10) degenerates to the purely poro-elastic model studied experimentally and analytically in (Soltz & Ateshian, 1998). Besides, the boundary and initial conditions (3.4.8) to (3.4.10) considered correspond to the creep experimental test performed in confined compression test.

Rewriting the system of equations (3.4.1) to (3.4.10) in terms of the derivatives of the solid displacement u the following apply:
First, by integrating both sides of (3.4.1), with respect to x yields

$$\frac{\partial u(x,t)}{\partial t} + v(x,t) = \eta(t), \tag{3.4.11}$$

where $\eta(t)$ is an arbitrary function of t. It follows from (3.4.8) that $\eta(t) = 0$, and thus (3.4.11) becomes

$$\begin{aligned} &\frac{\partial u(x,t)}{\partial t} + v(x,t) = 0 \\ \implies\ &v(x,t) = -\frac{\partial u(x,t)}{\partial t} \end{aligned} \tag{3.4.12}$$

Substituting (3.4.12) into (3.4.6) yields

$$\frac{\partial u}{\partial t} = K\frac{\partial p}{\partial x}, \tag{3.4.13}$$

so that (3.4.7) becomes

$$\frac{\partial u}{\partial t} - K\alpha\frac{\partial^2 u}{\partial x^2} - K\beta\frac{\partial^3 u}{\partial t \partial x^2} = 0. \tag{3.4.14}$$

Now using (3.4.2) and (3.4.3), it follows from (3.4.9) that

$$\begin{aligned} \sigma(L,t) = \sigma_e(L,t) + \delta\sigma_v(L,t) - p(L,t) &= -F(t) \\ \implies\ \alpha\frac{\partial u(L,t)}{\partial x} + \beta\frac{\partial^2 u(L,t)}{\partial x \partial t} &= -F(t). \end{aligned} \tag{3.4.15}$$

Therefore, the system (3.4.2) to (3.4.10) reduces to the following non-linear initial boundary

value problem (NLIBVP) which characterises a poro-viscoelastic medium in one-dimension:

$$\frac{\partial u}{\partial t} - K\alpha\frac{\partial^2 u}{\partial x^2} - K\beta\frac{\partial^3 u}{\partial t \partial x^2} = 0 \qquad \text{in} \quad (0, L) \times (0, T) \tag{3.4.16}$$

$$\alpha\frac{\partial u(L,t)}{\partial x} + \beta\frac{\partial^2 u(L,t)}{\partial x \partial t} = -F(t) \qquad 0 < t < T \tag{3.4.17}$$

$$u(0,t) = v(0,t) = 0 \qquad 0 < t < T \tag{3.4.18}$$

$$u(x,0) = 0 \qquad 0 < x < L \tag{3.4.19}$$

Setting $\beta = 0$ (absence of structural viscoelasticity in the medium), the system (3.4.16) to (3.4.19) reduces to

$$\frac{\partial u}{\partial t} - K\alpha\frac{\partial^2 u}{\partial x^2} = 0 \qquad \text{in} \quad (0, L) \times (0, T) \tag{3.4.20}$$

$$\alpha\frac{\partial u(L,t)}{\partial x} = -F(t) \qquad 0 < t < T \tag{3.4.21}$$

$$u(0,t) = v(0,t) = 0 \qquad 0 < t < T \tag{3.4.22}$$

$$u(x,0) = 0 \qquad 0 < x < L \tag{3.4.23}$$

and this corresponds to one-dimensional poro-elastic problem.

In addition to the system (3.4.2) to (3.4.10), this study considers an important quantity associated with fluid-solid mixture called the fluid power density $\mathcal{P}(t)$ which is the time rate of energy transfer per unit volume of fluid. In this case, $\mathcal{P}(t)$ is given by:

$$\mathcal{P}(t) = \frac{1}{K}\int_0^L v(x,t)^2 dx, \tag{3.4.24}$$

where K is the medium permeability and $v(x,t)$ is the discharge velocity.

3.5 Explicit solution of model

First, assume that the permeability is a non-zero positive real constant K_0, that's

$$K := K(x, \frac{\partial u}{\partial x}) \equiv K_0 > 0. \tag{3.5.1}$$

The system (3.4.16) to (3.4.19) becomes a linear initial non-homogeneous boundary value problem (LINHBVP). A formal solution $u(x,t)$ to the resulting linear system using Fourier series expansion techniques is as follows:

Homogenise the boundary conditions by setting

$$\varphi(x,t) = u(x,t) + G(x,t), \tag{3.5.2}$$

and supposing that for an auxilliary function $\mu(t)$

$$G(x,t) = \frac{\mu(t)}{\alpha}x, \tag{3.5.3}$$

which at $x = L$ satisfies

$$\alpha\frac{\partial G(L,t)}{\partial x} + \beta\frac{\partial^2 G(L,t)}{\partial x \partial t} = F(t). \tag{3.5.4}$$

Substituting (3.5.3) into (3.5.4) yields

$$\frac{d\mu(t)}{dt} + \frac{\alpha}{\beta}\mu(t) = \frac{\alpha}{\beta}F(t), \tag{3.5.5}$$

and by integrating factor techniques,

$$\mu(t) = \frac{\alpha}{\beta}\int_0^t \exp(-\frac{\alpha}{\beta}(t-s))F(s)ds = \frac{\alpha}{\beta}\exp(-\frac{\alpha}{\beta}t) \circledast F(t), \tag{3.5.6}$$

where $\circledast$ represents convolution. Hence, (3.5.2) becomes

$$\varphi(x,t) = u(x,t) + \frac{x}{\beta}\exp(-\frac{\alpha}{\beta}t) \circledast F(t), \tag{3.5.7}$$

which is the choice of function to homogenize the non-homogeneous problem. Therefore

$\varphi(x,t)$ satisfies the problem

$$\begin{cases} \dfrac{\partial \varphi}{\partial t} - K_0\alpha\dfrac{\partial^2\varphi}{\partial x^2} - K_0\beta\dfrac{\partial^3\varphi}{\partial t\partial x^2} = \dfrac{x}{\alpha}\mu'(t) & \text{in } \ (0,L)\times(0,T) \quad (3.5.8) \\ \alpha\dfrac{\partial\varphi(L,t)}{\partial x} + \beta\dfrac{\partial^2\varphi(L,t)}{\partial x\partial t} = 0 & 0<t<T \quad (3.5.9) \\ \varphi(0,t) = 0 & 0<t<T \quad (3.5.10) \\ \varphi(x,0) = 0 & 0<x<L, \quad (3.5.11) \end{cases}$$

where prime denotes the derivative of $\mu(t)$ with respect to t. Hence, the system (3.5.8) to (3.4.19) is a linear initial homogeneous boundary Value Problem and the associated eigenvalue problem is of the form:

$$y'' + \lambda y = 0, \ \ y(0) = y'(L) = 0, \quad 0<x<L, \tag{3.5.12}$$

To find numerical values for λ for which (3.5.12) has a non-trivial solution. This is possible when $\lambda > 0$. Let $\lambda = k^2, \ \ k \neq 0$. Then the general solution of (3.5.12) is

$$y(x) = a\cos kx + b\sin kx, \tag{3.5.13}$$

where a and b are arbitrary constants. When $x = 0$, $y(0) = 0 = a$, and for $x = L$, we get

$$y'(L) = 0 = b\cos kL.$$

For non-trivial solution $b \neq 0$ (for simplicity, $b = 1$), and so it must be that $\cos kL = 0$. This is true whenever

$$k = \frac{(2n-1)}{2L}\pi, \quad \forall n \in \mathbb{N}, \tag{3.5.14}$$

so that

$$\lambda_n := \lambda = k^2 = \frac{(2n-1)^2\pi^2}{4L^2}, \text{ and } \ y_n(x) = \sin\left(\frac{2n-1}{2L}\right)\pi x, \quad \forall n \in \mathbb{N} \tag{3.5.15}$$

where λ_n is the eigenvalues and $y_n(x)$ is the eigenvectors.

To the system of equations (3.5.8) to (3.5.11), a solution of the form

$$\varphi(x,t) = \sum_{n=1}^{\infty} a_n(t) y_n(x), \tag{3.5.16}$$

is to be obtained, where $y_n(x)$ is as computed in (3.5.15), and $a_n(t)$ is the series' coefficients to be determined. For $f(x) = x,\ 0 < x < L$, the Fourier series expansion is

$$f(x) = \frac{2}{L} \sum_{n=1}^{\infty} \frac{(-1)^{n-1}}{\lambda_n} y_n(x) \tag{3.5.17}$$

Substituting (3.5.16), and (3.5.17) into (3.5.8) yields

$$\sum_{n=1}^{\infty} a_n'(t) y_n(x) - K_0 \sum_{n=1}^{\infty} a_n(t) y_n''(x) - K_0 \beta \sum_{n=1}^{\infty} a_n'(t) y_n''(x) = \frac{2}{\alpha L} \sum_{n=1}^{\infty} \frac{(-1)^{n-1}}{\lambda_n} y_n(x) \mu'(t) \tag{3.5.18}$$

$$\implies \sum_{n=1}^{\infty} y_n(x) \Big[(1 + K_0 \beta \lambda_n) a_n'(t) + \alpha K_0 \lambda_n a_n(t) \Big] = \sum_{n=1}^{\infty} \frac{2(-1)^{n-1}}{\alpha L \lambda_n} y_n(x) \mu'(t). \tag{3.5.19}$$

Using the uniqueness of Fourier series expansion (O'Neil, 2011), it follows from (3.5.19) that for any $n \in \mathbb{N}$

$$(1 + K_0 \beta \lambda_n) a_n'(t) + \alpha K_0 \lambda_n a_n(t) = \frac{2(-1)^{n-1}}{\alpha L \lambda_n} \mu'(t), \tag{3.5.20}$$

which is a first order ODE in a_n, with initial condition $a_n(0) = 0$. By integrating factor techniques, we get

$$\begin{aligned} a_n(t) &= \frac{2(-1)^{n-1}}{\alpha L \lambda_n (1 + K_0 \beta \lambda_n)} \int_0^t \exp(-\frac{\alpha K_0 \lambda_n}{1 + K_0 \beta \lambda_n}(t-s)) \mu'(s) ds \\ &= \frac{2(-1)^{n-1}}{\alpha L \lambda_n (1 + K_0 \beta \lambda_n)} \exp(-\frac{\alpha K_0 \lambda_n}{1 + K_0 \beta \lambda_n} t) \circledast \mu'(t), \end{aligned} \tag{3.5.21}$$

so that (3.5.16) becomes

$$\varphi(x,t) = \sum_{n=1}^{\infty} \frac{2(-1)^{n-1} y_n(x)}{\alpha L \lambda_n (1 + K_0 \beta \lambda_n)} \exp(-\frac{\alpha K_0 \lambda_n}{1 + K_0 \beta \lambda_n} t) \circledast \mu'(t). \tag{3.5.22}$$

Substituting (3.5.22) into (3.5.7) yields

$$u(x,t) = -x\frac{\mu(t)}{\alpha} + \sum_{n=1}^{\infty} \frac{2(-1)^{n-1} y_n(x)}{\alpha L \lambda_n (1 + K_0 \beta \lambda_n)} \exp\Big(- \frac{\alpha K_0 \lambda_n}{1 + K_0 \beta \lambda_n} t\Big) \circledast \mu'(t)$$

$$\implies u(x,t) = -\frac{2}{\alpha L} \sum_{n=1}^{\infty} \frac{(-1)^{n-1} y_n(x)}{\lambda_n} \Bigg(\mu(t) - \frac{1}{(1 + K_0 \beta \lambda_n)} \int_0^t \exp\Big(- \frac{K_0 \alpha \lambda_n}{1 + K_0 \beta \lambda_n}(t-s)\Big) \mu'(s) ds \Bigg) \tag{3.5.23}$$

Taking (3.5.5) as identity coupled with integration by parts, then (3.5.23) can be rewritten as follows:

$$\begin{aligned} u(x,t) &= -\frac{2K_0}{L} \sum_{n=1}^{\infty} \frac{(-1)^{n-1} y_n(x)}{(1 + K_0 \beta \lambda_n)} \int_0^t \exp\Big(- \frac{K_0 \alpha \lambda_n}{1 + K_0 \beta \lambda_n}(t-s)\Big) F(s) ds \\ &= -\frac{2K_0}{L} \sum_{n=1}^{\infty} \frac{(-1)^{n-1} y_n(x)}{(1 + K_0 \beta \lambda_n)} \exp\Big(- \frac{K_0 \alpha \lambda_n}{1 + K_0 \beta \lambda_n} t\Big) \circledast F(t) \end{aligned} \tag{3.5.24}$$

The expression in (3.5.24) is the formal solution to the problem in (3.4.16) to (3.4.19), with medium permeability given by (3.5.1), and $\beta > 0$. When $\beta = 0$, (3.5.24) reduces to the formal solution of the problem in (3.4.20) to (3.4.23).

3.5.1 Well-posedness of the Weak Solution $u(x,t)$

This section shows that the solution $u(x,t)$ obtained for the case $\beta > 0$ actually solves the problem in (3.4.16) to (3.4.19) in a well-defined functional space. The symbol $H^k(\Omega)$ for $\Omega \subset \mathbb{R}^n$ open and for any integer $k \geq 0$ denotes the usual real Sobolev space,

$$H^k(\Omega) = \{v \in \mathcal{L}^2(\Omega) : D^i v \in \mathcal{L}^2(\Omega) \; \forall |i| \leq k\}$$

equipped with the norm

$$\|v\|_k = \sqrt{\sum_{|i|\leq k} \|D^i v\|^2_{\mathcal{L}^2(\Omega)}}$$

where $D^i v$ is the $i^{th}-$weak derivative of v. For real number $1 \leq p < \infty$, $\mathcal{L}^p(\Omega)$ denotes the space of strongly measurable continuous functions f on Ω such that the norm

$$\|f\|_{\mathcal{L}^p(\Omega)} = \Big(\int_\Omega |f|^p \Big)^{\frac{1}{p}} < \infty,$$

and for $p = \infty$ the norm is given by

$$\|f\|_{\mathcal{L}^\infty(\Omega)} = \max_{\vec{x}\in\Omega} f(\vec{x})$$

(Brezis, 2010; Holzapfel & Ogden, 2017). For $\Omega = (0, L) \subset \mathbb{R}$, consider the real Sobolev space H given by

$$H := H^0(0, L) = \mathcal{L}^2(0, L),$$

which is a Hilbert space when equipped with an inner product

$$\langle f, g \rangle_H = \int_0^L fg dx \quad \forall f, g \in H. \tag{3.5.25}$$

This inner product induces the norm

$$\|f\|_H = \Big(\int_0^L f^2 dx \Big)^{\frac{1}{2}} = \sqrt{\langle f, f \rangle_H}, \tag{3.5.26}$$

so that $\big(H,\ \|\cdot\|_H\big)$ becomes a Banach Space (Brezis, 2010).

On the application of Gram-Schmidt Process to the linearly independent set $\{y_n(x)\}_{n=1}^\infty$ we obtain the orthonormal sequence $\mathcal{C} = \{\sqrt{\frac{2}{L}} y_n(x)\}_{n=1}^\infty$ in H (Bowers & Kalton, 2014). Clearly, it follows from the linear independence property of orthonormal sequence that $\mathcal{C}$ span the inner product space H.

Theorem 3.5.1. Let $\{e_k\}$ be an orthonormal sequence in a Hilbert space H.

a) The series

$$\sum_{k=1}^{\infty} c_k e_k, \quad c_k \text{ scalars}$$

converges in the norm on H if and only if the following series

$$\sum_{k=1}^{\infty} |c_k|^2$$

converges, that's

$$\sum_{k=1}^{\infty} |c_k|^2 < \infty.$$

b) If (a) is true then the coefficients c_k are the Fourier coefficient $\langle x, e_k \rangle_H$, where

$$x = \sum_{k=1}^{\infty} c_k e_k \quad \text{in } H$$

(Ovchinnikov, 2018).

Proof. a) Assume that the series $\sum_{k=1}^{\infty} c_k e_k$, c_k scalars converges, with sum x. Then let

$$s_n = c_1 e_1 + c_2 e_2 + ... + c_n e_n \tag{3.5.27}$$

be the nth partial sums such that $\|s_n - x\|_H \to 0$ as $n \to \infty$. Let

$$\sigma_n = |c_1|^2 + |c_2|^2 + ... + |c_n|^2. \tag{3.5.28}$$

For any $n, m \in \mathbb{N}$, with $n > m$, it follows from (3.5.27) that

$$\begin{aligned} \|s_n - s_m\|_H &= \|c_{m+1} e_{m+1} + c_{m+2} e_{m+2} + ... + c_n e_n\|_H \\ \implies \|s_n - s_m\|_H^2 &= \|c_{m+1} e_{m+1} + c_{m+2} e_{m+2} + ... + c_n e_n\|_H^2 \\ \implies \|s_n - s_m\|_H^2 &= \left\langle c_{m+1} e_{m+1} + ... + c_n e_n,\, c_{m+1} e_{m+1} + ... + c_n e_n \right\rangle_H \end{aligned} \tag{3.5.29}$$

Using the property of orthonormal sequence and (3.5.28), then (3.5.29) yields

$$\begin{aligned}\|s_n - s_m\|_H^2 &= |c_{m+1}|^2 + |c_{m+1}|^2 + ... + |c_n|^2 \\ &= \sigma_n - \sigma_m, \quad \forall n > m. \end{aligned} \tag{3.5.30}$$

Hence the sequence $\{s_n\}_{n=1}^{\infty}$ is a Cauchy sequence in H, if and only if $\{\sigma_n\}_{n=1}^{\infty}$ is Cauchy in $\mathbb{C}$. Since H and $\mathbb{C}$ are complete, then (a) is true.

b) Assume that (a) is true. Taking inner product of s_n defined in (3.5.27) and e_j, we get

$$\langle s_n, e_j\rangle_H = \Big\langle c_1e_1 + c_2e_2 + ... + c_ne_n,\, e_j \Big\rangle_H = c_j, \quad j = 1, 2, ..., k \tag{3.5.31}$$

with $k \leq n$ fixed. By assumption

$$s_n \to x, \quad \text{as } \; n \to \infty,$$

and since inner product is continuous, then

$$\begin{aligned} c_j = \langle s_n, e_j\rangle_H &\to \langle x, e_j\rangle_H \\ \implies c_j = \langle x, e_j\rangle_H, &\;\; j = 1, 2, ... \end{aligned} \tag{3.5.32}$$

which are the required Fourier coefficients.

□

Definition 3.5.2. Let $\mathcal{C}_0^{\infty}(0, L)$ be the space of test functions on $(0, L)$. A distribution v on $(0, L)$ is a linear functional

$$v : \mathcal{C}_0^{\infty}(0, L) \longrightarrow \mathbb{C},$$

with the following continuity property; $f_n \longrightarrow f$ in $\mathcal{C}_o^{\infty}(0, L)$ implies that $v(f_n) \longrightarrow v(f)$ in $\mathbb{C}$. Here, the space of distributions on $(0, L)$ is denoted by $\mathcal{D}'(0, L)$ (Haroske & Triebel, 2008).

Using the basis $\mathcal{C}$ for H, it follows from Theorem (3.5.1) that any $v \in \mathcal{D}'(0, L)$ belongs to H if

and only if

$$v(x) = \sum_{n=1}^{\infty} c_n y_n(x) \tag{3.5.33}$$

(converging in $\mathcal{D}'(0, L)$), with the scalars c_n satisfying

$$\sum_{n=0}^{\infty} |c_n|^2 < \infty.$$

Further, let

$$\mathcal{V} = \{v \in H : v' \text{ exist, } v' \in H \text{ and } v(0) = 0\},$$

and equip $\mathcal{V}$ with the inner product

$$\langle f, g\rangle_{\mathcal{V}} = \langle f', g'\rangle_H, \quad \forall f, g \in \mathcal{V}. \tag{3.5.34}$$

Clearly, the space $(\mathcal{V}, \langle\cdot,\cdot\rangle_{\mathcal{V}})$ is a Hilbert space. By Poincaire Inequality (Marin & Öchsner, 2018), the norm $\|\cdot\|_{\mathcal{V}}$ becomes

$$\|v\|_{\mathcal{V}} = \|v'\|_H, \quad \forall v \in \mathcal{V}. \tag{3.5.35}$$

As a consequence of Sobolev's inequality, $v \in \mathcal{V}$ implies that $v \in AC([0, L])$, the space of absolutely continuous function, so that the boundary condition $v(0) = 0$ is assumed in the strong sense.

The sequence $\left\{\sqrt{\frac{2}{L\lambda_n}} y_n(x)\right\}_{n=1}^{\infty}$ is a Hilbert basis for $\mathcal{V}$, and any $v \in H$ is in $\mathcal{V}$ if the Fourier coefficients of its series expansion in (3.5.33) satisfies

$$\sum_{n=1}^{\infty} \lambda_n |c_n|^2 < \infty.$$

Therefore, for any $s \in \mathbb{R}$, we define a one-paremeter family of spaces, $\mathcal{V}^s$ as

$$\mathcal{V}^s = \{v \in \mathcal{D}'(0, L) : \exists\, a_k \in \mathbb{C},\ v(x) = \sum_{k=1}^{\infty} a_k y_n(x),\ \text{provided } \sum_{k=1}^{\infty} \lambda_k^s |c_k|^2 < \infty\}.$$

Next, the definition of a weak solution for the problem in (3.4.16) to (3.4.19) when $\beta > 0$ is as follows:

Definition 3.5.3. A function

$$u : [0, L] \times [0, T] \longrightarrow \mathcal{V}$$
$$(x, t) \longmapsto u(x, t) := u$$

is a weak solution to problem (3.4.16) to (3.4.19) if

i) $u \in H^1([0, L] \times [0, T]; \mathcal{V})$, implies that $u, \frac{\partial u}{\partial t} \in \mathcal{L}^2([0, L] \times [0, T]; \mathcal{V})$

ii) For any $v \in \mathcal{V}$, and $t \in [0, T]$ pointwise almost everywhere, then

$$\Big\langle \frac{\partial u}{\partial t}, v \Big\rangle_H + K_0 \Big\langle \alpha u + \beta \frac{\partial u}{\partial t}, v \Big\rangle_{\mathcal{V}} = -K_0 F(t) v(L) \tag{3.5.36}$$

iii) $u(x, 0) = 0$

The initial condition (3.4.19) is satisfied by $u(x, t) \in \mathcal{V}$ in the pointwise sense according to condition (iii), since condition (i) implies that $u \in AC([0, L] \times [0, T]; \mathcal{V})$ (Keener, 2018). The boundary condition in (3.4.18) is included in the requirement that $u \in \mathcal{V}$, and the boundary condition (3.4.17) is taking into account by condition (ii) for any test function $v \in \mathcal{V}$.
Now, the condition for the well-posedness of the solution $u(x, t)$ is provided in the next theorem.

Main Theorem 3.5.1. Assume that $F(t) \in \mathcal{L}^2(0, T)$. Then there exist a unique weak solution u according to Definition (3.5.3). to problem (3.4.16) to (3.4.19). The series expansion of u is given in (3.5.24).

Proof. First, we re-express $u(x, t)$ in (3.5.24) as

$$u(x, t) = \sum_{n=1}^{\infty} u_n(t) y_n(x), \tag{3.5.37}$$

where

$$u_n(t) = -2 \frac{K_0 (-1)^{n-1}}{L(1 + K_0 \beta \lambda_n)} \exp\Big(- \frac{K_0 \alpha \lambda_n}{1 + K_0 \beta \lambda_n} t \Big) \circledast F(t), \quad n \in \mathbb{N}. \tag{3.5.38}$$

From (3.5.37),

$$\frac{\partial u(x,t)}{\partial t} = \sum_{n=1}^{\infty} u_n'(t) y_n(x), \tag{3.5.39}$$

with

$$\begin{aligned} u_n'(t) = \frac{du_n(t)}{dt} &= \frac{-2K_0(-1)^{n-1}}{L(1+K_0\beta\lambda_n)}\left[F(t) - \frac{K_0\alpha\lambda_n}{1+K_0\beta\lambda_n}\exp\Big(-\frac{K_0\alpha\lambda_n}{1+K_0\beta\lambda_n}t\Big) \circledast F(t)\right] \\ &= \frac{-2K_0(-1)^{n-1}}{L(1+K_0\beta\lambda_n)}F(t) - \frac{K_0\alpha\lambda_n}{1+K_0\beta\lambda_n}u_n(t), \quad n \in \mathbb{N}. \end{aligned} \tag{3.5.40}$$

Now, to show that u has the required regularity, that's $u \in H^1([0,L]\times[0,T];\mathcal{V})$ and $u(x,0) = 0$. First, the convergence of (3.5.38) and (3.5.40) is studied as follows. For every $c > 0$,

$$\begin{aligned} |\exp(-ct) \circledast F(t)| &= \Big|\int_0^t \exp[-c(t-s)]F(s)ds\Big| \quad \text{(By definition of convolution)} \\ &\leq \Big(\int_0^t (\exp[-c(t-s)])^2 ds\Big)^{\frac{1}{2}}\Big(\int_0^t |F(s)|^2 ds\Big)^{\frac{1}{2}} \quad \text{(By Cauchy-Schwartz inequality)} \\ &\leq \frac{1}{\sqrt{2c}}\|F\|_{\mathcal{L}^2(0,T)} \\ \implies |\exp(-ct) \circledast F(t)| &\leq \frac{1}{\sqrt{2c}}\|F\|_{\mathcal{L}^2(0,T)}, \end{aligned} \tag{3.5.41}$$

Using (3.5.41), it follows from (3.5.38) that

$$|u_n(t)| \leq \frac{D}{\lambda_n}\|F\|_{\mathcal{L}^2(0,T)}, \tag{3.5.42}$$

and from (3.5.40),

$$|u_n'(t)| \leq \frac{D}{\lambda_n}\Big(|F(t)| + \|F\|_{\mathcal{L}^2(0,T)}\Big), \tag{3.5.43}$$

where D is a constant independent of n and t. Therfore, $u(x,t), \frac{\partial u(x,t)}{\partial t} \in \mathcal{L}^2([0,L]\times[0,T];\mathcal{V}^s)$, for $s < \frac{3}{2}$ and as such, conditions (i) and (iii) of Definition (3.5.3) are satisfied.

Next, to show that $u(x,t)$ satisfies condition (ii), let $v = y_n(x),\ n \in \mathbb{N}$ be a test function. Each

term on the left handside of (ii) becomes

$$\begin{aligned}\Big\langle \frac{\partial u}{\partial t}, y_n \Big\rangle_H &= \int_0^L \frac{\partial u}{\partial t} y_n(x)dx = \int_0^L \sum_{m=1}^{\infty} u_m'(t) y_m(x) y_n(x)dx \\ &= \int_0^L u_n'(t) y_n^2(x)dx, \quad \Big(\text{since } \int_0^L y_n(x)y_m(x)dx = 0,\ \forall n \neq m\Big). \\ &= \frac{L}{2} u_n'(t), \end{aligned} \tag{3.5.44}$$

$$\begin{aligned}\langle u, y_n\rangle_{\mathcal{V}} = \Big\langle \frac{\partial u}{\partial x}, \frac{\partial y_n(x)}{\partial x} \Big\rangle_H &= \int_0^L \frac{\partial u}{\partial x}\frac{\partial y_n(x)}{\partial x}dx \\ &= \int_0^L \sum_{m=1}^{\infty} u_m(t)\frac{\partial y_m(x)}{\partial x}\frac{\partial y_n(x)}{\partial x}dx \\ &= u_n(t)\lambda_n \int_0^L \cos^2\Big(\frac{2n-1}{2L}\Big)\pi x dx \\ &= \frac{L\lambda_n}{2} u_n(t), \end{aligned} \tag{3.5.45}$$

and

$$\begin{aligned}\Big\langle \frac{\partial u}{\partial t}, y_n \Big\rangle_{\mathcal{V}} = \Big\langle \frac{\partial^2 u}{\partial x \partial t}, \frac{\partial y_n(x)}{\partial x} \Big\rangle_H &= \int_0^L \frac{\partial^2 u}{\partial x \partial t}\frac{\partial y_n(x)}{\partial x}dx \\ &= \int_0^L \sum_{m=1}^{\infty} \frac{\partial u_m(t)}{\partial t}\frac{\partial y_m(t)}{\partial x}\frac{\partial y_n(t)}{\partial x}dx \\ &= \frac{L\lambda_n}{2} u_n'(t), \end{aligned} \tag{3.5.46}$$

so that

$$\begin{aligned}\Big\langle \frac{\partial u}{\partial t}, y_n(x) \Big\rangle_H + K_0\Big\langle \alpha u + \beta\frac{\partial u}{\partial t}, y_n(x)\Big\rangle_{\mathcal{V}} &= \Big\langle \frac{\partial u}{\partial t}, y_n(x) \Big\rangle_H + K_0\Big\langle \alpha u, y_n(x)\Big\rangle_{\mathcal{V}} + K_0\Big\langle \beta\frac{\partial u}{\partial t}, y_n(x)\Big\rangle_{\mathcal{V}} \\ &= \frac{L}{2}u_n'(t) + \frac{LK_0\alpha\lambda_n}{2}u_n(t) + \frac{LK_0\lambda_n\beta}{2}u_n'(t) \\ &= \frac{L}{2}\Big(u_n'(t)(1+K_0\beta\lambda_n) + K_0\lambda_n u_n(t)\Big) \end{aligned} \tag{3.5.47}$$

By substituting (3.5.40) into (3.5.47) with the fact that $y_n(L) = (-1)^{n-1},\ \forall n \in \mathbb{N}$, yields

$$\Big\langle \frac{\partial u}{\partial t}, y_n(x) \Big\rangle_H + K_0\Big\langle \alpha u + \beta\frac{\partial u}{\partial t}, y_n(x)\Big\rangle_{\mathcal{V}} = -F(t)K_0 y_n(L), \tag{3.5.48}$$

the righthandside of condition (ii). Thus condition (ii) is proved and it implies the proof of existence of solution.

Finally, to prove the uniqueness of solution. Since we are dealing with a linear PDEs, it is sufficient to show that $F = 0$, implies that $u = 0, \forall t \in [0, T]$. Suppose that $F = 0$, and let $u \in H^1([0, L] \times [0, T]; \mathcal{V})$ be a solution of

$$\Big\langle \frac{\partial u}{\partial t}, v \Big\rangle_H + K_0 \Big\langle \alpha u + \beta \frac{\partial u}{\partial t}, v \Big\rangle_{\mathcal{V}} = 0, \qquad v \in \mathcal{V}. \tag{3.5.49}$$

Let $v = u$ be a test function, then (3.5.49) reduces to

$$\begin{aligned} \Big\langle \frac{\partial u}{\partial t}, u \Big\rangle_H + K_0 \Big\langle \alpha u + \beta \frac{\partial u}{\partial t}, u \Big\rangle_{\mathcal{V}} &= 0 \\ \implies \int_0^L \frac{\partial u}{\partial t} u dx + K_0 \beta \int_0^L \frac{\partial u}{\partial t} u dx &= -K_0 \alpha \int_0^L u^2 dx \\ \implies \frac{\partial}{\partial t} \Big(\|u\|_H^2 + K_0 \beta \|u\|_{\mathcal{V}}^2 \Big) &= -K_0 \alpha \|u\|_{\mathcal{V}}^2 \leq 0 \\ \implies \frac{\partial}{\partial t} \Big(\|u\|_H^2 + K_0 \beta \|u\|_{\mathcal{V}}^2 \Big) &\leq 0 \end{aligned} \tag{3.5.50}$$

Integrating both sides of (3.5.50) with respect to t and taking the initial condition $u(x, 0) = 0$ we obtain

$$\|u\|_H^2 + K_0 \beta \|u\|_{\mathcal{V}}^2 \leq 0.$$

Thus, $u = 0 \quad \forall t \in [0, T]$. □

Using the fact that $|y_n(x)| \leq 1, \quad \forall n \in \mathbb{N}$, and the estimate in (3.5.42), it follows from Weierstrass M-test that the series in (3.5.37) converges absolutely and uniformly in $[0, L] \times [0, T]$ and its sum $u(x, t)$ is continuous. Similarly, by using the strong assumption that $F(t) \in \mathcal{L}^\infty(0, T)$, it is found that the series in (3.5.39) also converges absolutely and uniformly in $[0, L] \times [0, T]$ so that its sum $\frac{\partial u}{\partial t}$ is continuous. Therefore, in a physical situation where the boundary traction is bounded, fluid discharge velocity is continuous and bounded both in space and time and using (3.4.24) implies that the power density is also continuous and bounded both in space and time, even when there are point of discontinuity in the boundary traction.

3.6 Dimensionless Form of Problem

In this section, dimensional analysis is used to provide the equivalence of problem (3.4.16) to (3.4.19) in dimensionless form so as to identify the combinations of geometrical and physical parameters that most influence the solution properties. Dimensional analysis is a mathematical technique that leans on the choice of a set of characteristic values that can be used to scale all variables in the problem. Here, the hat symbols denote scaled (dimensionless) variables, and the square bracket denotes characteristic values of the variable. Then

$$\begin{cases} \hat{t} = \dfrac{t}{[t]} \qquad \hat{x} = \dfrac{x}{[x]} \qquad \hat{\beta} = \dfrac{\beta}{[\beta]} \qquad \hat{\lambda}_n = \dfrac{\lambda_n}{[\lambda_n]} \\ \\ \hat{\mathcal{P}} = \dfrac{\mathcal{P}}{[\mathcal{P}]} \qquad \hat{F} = \dfrac{F}{[F]} \qquad \hat{u} = \dfrac{u}{[u]} \qquad \hat{v} = \dfrac{v}{[v]}. \end{cases} \tag{3.6.1}$$

It is crucial to note that there is no trivial selection for the characteristic values, and so this choice is not unique. In this case, the knowledge of the forcing term and the explicit solution obtained will help in the selection of these values.

3.6.1 Choice of characteristic values

Since the physical system is driven by the boundary condition on the forcing term with the given function $F(t)$, put

$$[F] = F_{\text{spec}}, \tag{3.6.2}$$

where F_{spec} is a given reference value. Following the expression in (3.5.15), choose

$$[x] = L, \qquad [\lambda_n] = \frac{1}{L^2}. \tag{3.6.3}$$

From the explicit formula obtained for the solution set

$$[\beta] = \frac{L^2}{K_0}, \quad [t] = \frac{[K_0][\beta][\lambda_n]}{[K_0][\alpha][\lambda_n]} = \frac{[\beta]}{\alpha} = \frac{L^2}{K_0\alpha}, \quad [u] = \frac{[K_0][F][t]}{[L]} = \frac{F_{\text{spec}}L}{\alpha} \tag{3.6.4}$$

According to (3.4.12), and (3.4.24) select for

$$[v] = \frac{[u]}{[t]} = \frac{K_0 F_{\text{spec}}}{L}, \qquad [\mathcal{P}] = \frac{[L][v]^2}{[K_0]} = \frac{K_0 F_{\text{spec}}}{L}. \tag{3.6.5}$$

By chain rule and (3.6.1) yield

$$\frac{\partial u}{\partial t} = \frac{\partial u}{\partial \hat{u}} \cdot \frac{\partial \hat{u}}{\partial \hat{t}} \cdot \frac{\partial \hat{t}}{\partial t} = \frac{[u]}{[t]} \frac{\partial \hat{u}}{\partial \hat{t}}, \tag{3.6.6}$$

$$\frac{\partial u}{\partial x} = \frac{\partial u}{\partial \hat{u}} \cdot \frac{\partial \hat{u}}{\partial \hat{x}} \cdot \frac{\partial \hat{x}}{\partial x} = \frac{[u]}{[x]} \frac{\partial \hat{u}}{\partial \hat{x}}, \tag{3.6.7}$$

$$\frac{\partial^2 u}{\partial x^2} = \frac{\partial}{\partial x}\Big(\frac{\partial u}{\partial x}\Big) = \frac{\partial}{\partial \hat{x}}\Big(\frac{[u]}{[x]} \frac{\partial \hat{u}}{\partial \hat{x}}\Big) \frac{\partial \hat{x}}{\partial x} = \frac{[u]}{[x]^2} \frac{\partial^2 \hat{u}}{\partial \hat{x}^2}, \tag{3.6.8}$$

$$\frac{\partial^2 u}{\partial t \partial x} = \frac{\partial}{\partial t}\Big(\frac{\partial u}{\partial x}\Big) = \frac{\partial}{\partial \hat{t}}\Big(\frac{[u]}{[x]} \frac{\partial \hat{u}}{\partial \hat{x}}\Big) \frac{\partial \hat{t}}{\partial t} = \frac{[u]}{[x][t]} \frac{\partial^2 \hat{u}}{\partial \hat{t} \partial \hat{x}}, \tag{3.6.9}$$

and

$$\frac{\partial^3 u}{\partial x^2 \partial t} = \frac{\partial}{\partial t}\Big(\frac{\partial^2 u}{\partial x^2}\Big) = \frac{\partial}{\partial \hat{t}}\Big(\frac{[u]}{[x]^2} \frac{\partial^2 \hat{u}}{\partial \hat{x}^2}\Big) \frac{\partial \hat{t}}{\partial t} = \frac{[u]}{[x]^2[t]} \frac{\partial^3 \hat{x}}{\partial \hat{u}^2 \partial t} \tag{3.6.10}$$

Substituting (3.6.6) to (3.6.10) and the scalings in (3.6.2) to (3.6.5) into the problem (3.4.16) to (3.4.19) yields the following dimensionless problem

$$\begin{cases} \dfrac{\partial \hat{u}}{\partial \hat{t}} - \dfrac{\partial^2 \hat{u}}{\partial \hat{x}^2} - \hat{\beta} \dfrac{\partial^3 \hat{u}}{\partial \hat{t} \partial \hat{x}^2} = 0 & \text{in} \quad (0,1) \times (0, \hat{T}) \qquad (3.6.11) \\ \dfrac{\partial \hat{u}(1,\hat{t})}{\partial \hat{x}} + \hat{\beta} \dfrac{\partial^2 \hat{u}(1,\hat{t})}{\partial \hat{x} \partial \hat{t}} = -\hat{F} & 0 < \hat{t} < \hat{T} \qquad (3.6.12) \\ \hat{u}(0,\hat{t}) = 0 & 0 < \hat{t} < \hat{T} \qquad (3.6.13) \\ \hat{u}(\hat{x},0) = 0 & 0 < \hat{x} < 1, \qquad (3.6.14) \end{cases}$$

where $\hat{T} = T[t]$. Using the scaling system, the dimensionless form of the solid displacement $u(x,t)$ in (3.5.24) becomes

$$\hat{u}(\hat{x},\hat{t}) = -2 \sum_{n=1}^{\infty} \frac{(-1)^{n-1} y_n(\hat{x})}{1 + \hat{\beta}\hat{\lambda}_n} \exp\Big(- \frac{\hat{\lambda}_n}{1 + \hat{\beta}\hat{\lambda}_n} \hat{t} \Big) \circledast \hat{F}(\hat{t}), \tag{3.6.15}$$

the dimensionless form of discharge velocity in (3.4.12) yields

$$\hat{v}(\hat{x},\hat{t}) = -\frac{\partial \hat{u}(\hat{x},\hat{t})}{\partial \hat{t}} = 2\sum_{n=1}^{\infty} \frac{(-1)^{n-1} y_n(\hat{x})}{1+\hat{\beta}\hat{\lambda}_n} \Big(\hat{F}(\hat{t}) - \frac{\hat{\lambda}_n}{1+\hat{\beta}\hat{\lambda}_n} \exp\Big(-\frac{\hat{\lambda}_n}{1+\hat{\beta}\hat{\lambda}_n}\hat{t}\Big) \circledast \hat{F}(\hat{t})\Big), \tag{3.6.16}$$

and the dimensionless form of the fluid power density in (3.4.24) is obtained as

$$\begin{aligned}
\hat{\mathcal{P}}(\hat{t}) &= \int_0^1 \hat{v}(\hat{x},\hat{t})^2 d\hat{x} \\
&= 2\sum_{n=1}^{\infty}\sum_{m=1}^{\infty} \frac{1}{(1+\hat{\beta}\hat{\lambda}_n)^2} \int_0^1 y_n(\hat{x}) y_m(\hat{x}) d\hat{x} \left(\hat{F}(\hat{t}) - \frac{\hat{\lambda}_n}{1+\hat{\beta}\hat{\lambda}_n} \exp\Big(-\frac{\hat{\lambda}_n}{1+\hat{\beta}\hat{\lambda}_n}\hat{t}\Big) \circledast \hat{F}(\hat{t}) \right)^2 \\
&= 2\sum_{n=1}^{\infty} \frac{1}{(1+\hat{\beta}\hat{\lambda}_n)^2} \left(\hat{F}(\hat{t}) - \frac{\hat{\lambda}_n}{1+\hat{\beta}\hat{\lambda}_n} \exp\Big(-\frac{\hat{\lambda}_n}{1+\hat{\beta}\hat{\lambda}_n}\hat{t}\Big) \circledast \hat{F}(\hat{t}) \right)^2
\end{aligned} \tag{3.6.17}$$

The characteristic value that is chosen for velocity in (3.6.5) is the characteristic velocity induced by the external load of magnitude F_{spec} which is in contrast to what was utilized in (Soltz & Ateshian, 1998). The justification is that the present study is interested in accessing the influence of an external load on the poromechanical response of the medium.

The next two sections consider the effects of two different types of dimensionless boundary tractions on the solutions obtained in (3.6.15) to (3.6.17).

3.6.2 Dimensionless unit Step-Pulse Load $\hat{F}(\hat{t})$

Here, suppose that the forcing term (boundary traction) $\hat{F}(\hat{t})$ is the dimensionless unit step function defined by

$$\hat{F}(\hat{t}) = H(\hat{t}) = \begin{cases} 0, & \text{if } \hat{t} < 0 \\ 1, & \text{if } \hat{t} \geq 0 \end{cases} \tag{3.6.18}$$

At the start of time $\hat{t} = 0$, there is discontinuity in the dimensionless load $\hat{F}(\hat{t})$ as shown in Fig.(3.2). Using (3.6.18), then (3.6.15), (3.6.16), and (3.6.17) respectively become

$$\hat{u}_{\hat{\beta}}(\hat{x},\hat{t}) = -2\sum_{n=1}^{\infty} \frac{(-1)^{n-1} y_n(\hat{x})}{\hat{\lambda}_n} \Big(1 - \exp\Big(-\frac{\hat{\lambda}_n}{1+\hat{\beta}\hat{\lambda}_n}\hat{t}\Big)\Big), \tag{3.6.19}$$

$$\hat{v}_{\hat{\beta}}(\hat{x},\hat{t}) = 2\sum_{n=1}^{\infty} \frac{(-1)^{n-1} y_n(\hat{x})}{1+\hat{\beta}\hat{\lambda}_n} \exp\Big(-\frac{\hat{\lambda}_n}{1+\hat{\beta}\hat{\lambda}_n}\hat{t}\Big), \tag{3.6.20}$$

and

$$\hat{\mathcal{P}}_{\hat{\beta}}(\hat{t}) = 2\sum_{n=1}^{\infty} \frac{1}{(1+\hat{\beta}\hat{\lambda}_n)^2} \exp\Big(-\frac{\lambda_n}{1+\hat{\beta}\hat{\lambda}_n}\hat{t}\Big)^2. \tag{3.6.21}$$

Setting $\hat{\beta} = 0$, in equations (3.6.19) to (3.6.21), result to the dimensionless solutions $\hat{u}_0,\ \hat{v}_0,$ and $\mathcal{P}_0$ for the dimensionless purely elastic problem respectively.

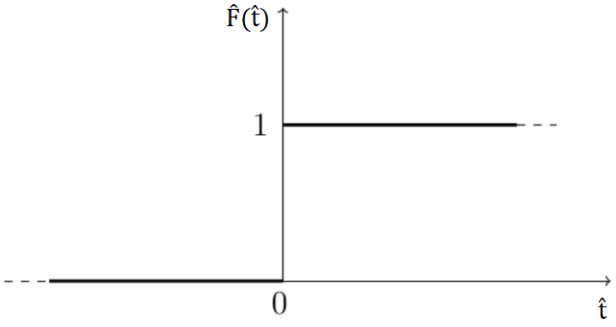

Figure 3.2. Diagrammatic representation of $\hat{F}(\hat{t})$

When viscoelasticity is absent, i.e. $\hat{\beta} = 0$, in the porous medium at the start of time $\hat{t} = 0$, then (3.6.20) and (3.6.21) (substituting $\hat{\beta} = \hat{t} = 0$,) yield

$$\hat{\mathcal{P}}_0(0) = 2\sum_{n=1}^{\infty} 1 = +\infty, \tag{3.6.22}$$

and

$$\hat{v}_0(\hat{x},0) = 2\sum_{n=1}^{\infty} (-1)^{n-1} y_n(\hat{x}). \tag{3.6.23}$$

respectively. In equation (3.6.23), for any $n \in \mathbb{N}$,

$$-1 \leq y_n(\hat{x}) \leq 1$$

and hence equation (3.6.23) lacks pointwise convergence. Suppose that viscoelasticity effect is present, i.e. $\hat{\beta} \neq 0$ then the dimensionless discharge velocity at the start of time $\hat{t} = 0$ (putting

$\hat{t} = 0$ in (3.6.20)) becomes

$$\hat{v}_{\hat{\beta}}(\hat{x}, 0) = 2\sum_{n=1}^{\infty} \frac{(-1)^{n-1} y_n(\hat{x})}{1 + \hat{\beta}\hat{\lambda}_n} \tag{3.6.24}$$

Substituting the expression for λ_n in (3.5.15) into (3.6.24) gives

$$\hat{v}_{\hat{\beta}}(\hat{x}, 0) = 2\sum_{n=1}^{\infty} \frac{(-1)^{n-1} y_n(\hat{x})}{1 + \hat{\beta}\left(\frac{2n-1}{2L}\right)^2 \pi^2} = 8L^2 \sum_{n=1}^{\infty} \frac{(-1)^{n-1} y_n(\hat{x})}{an^2 - an + b}, \tag{3.6.25}$$

where $a = 4\hat{\beta}\pi^2$, and $b = 4L^2 + \hat{\beta}\pi^2$ and using Alternating series test (Erdman, 2018), it is seen that the series in (3.6.25) is convergent. Also, it is continuous at $\hat{t} = 0$.

When $\hat{x} = 1$ and $\hat{t} = 0$, the maximum value of $\hat{v}_{\hat{\beta}}$, here denoted by $\hat{v}_{max}(\hat{\beta})$ is attained, and it's given by

$$\hat{v}_{max}(\hat{\beta}) = \max_{0 \le \hat{x} \le 1} |\hat{v}_{\hat{\beta}}(\hat{x}, \hat{t})| = \hat{v}_{\hat{\beta}}(1, 0) = 2\sum_{n=1}^{\infty} \frac{1}{1 + \hat{\beta}\hat{\lambda}_n}, \tag{3.6.26}$$

which depends on the structural viscoelasticity and lacks convergence. It is seen from (3.6.21) that the power density is decreasing with increase in time and its maximum value, $\hat{\mathcal{P}}_{\max}(\hat{\beta})$ is attained at $\hat{t} = 0$, that's

$$\hat{\mathcal{P}}_{max}(\hat{\beta}) = \max_{\hat{t} \le 0} |\hat{\mathcal{P}}_{\hat{\beta}}(\hat{t})| = \hat{v}_{\hat{\beta}}(1, 0) = 2\sum_{n=1}^{\infty} \frac{1}{(1 + \hat{\beta}\hat{\lambda}_n)^2}. \tag{3.6.27}$$

It is important to note from the definition of $\hat{\beta}$ that it does depend uniquely on the viscoelastic coefficients (see equations (3.6.1), and (3.6.4)). That's small or large value of the medium permeability K_0 and small or large value of the domain dimension L would have effect on the value of $\hat{\beta}$. Using the analysis in (3.6.1), and (3.6.5) then

$$\begin{cases} v_{\max}(\hat{\beta}) = \hat{v}_{\max}(\hat{\beta})[v] = \dfrac{F_{spec} K_0}{L} \hat{v}_{\max}(\hat{\beta}) \\ \\ \mathcal{P}_{\max}(\hat{\beta}) = \hat{\mathcal{P}}_{\max}(\hat{\beta})[\mathcal{P}] = \dfrac{F_{spec}^2 K_0}{L} \hat{\mathcal{P}}_{\max}(\hat{\beta}). \end{cases} \tag{3.6.28}$$

From (3.6.28), it can be seen that larger magnitude of the forcing term F_{spec} will give larger

value of $v_{\max}$ and $\mathcal{P}_{\max}$ respectively, with $\hat{\beta} = \frac{K_0}{L^2}\beta$ (this follows by substituting the expression for $[\beta]$ in (3.6.4) into the expression for $\hat{\beta}$ in (3.6.1)).

3.6.3 Dimensionless Trapezoidal-Pulse forcing term $\hat{F}(\hat{t})$

Here, a forcing term $\hat{F}(\hat{t})$ which is given by a dimensionless trapezoidal pulse of amplitude $a > 0$, in which switching on and off of the signal are characterized by linear ramp functions is considered.

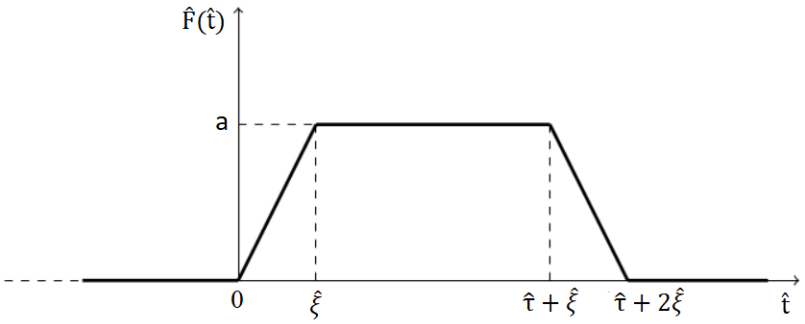

Figure 3.3. Diagrammatic representation of dimensionless $\hat{F}(\hat{t})$.

Let $\hat{\xi}, \hat{\tau} \in \mathbb{R}$, be positive, then take

$$\hat{F}(\hat{t}) = \begin{cases} 0, & \text{if } \hat{t} < 0 \\ \frac{a\hat{t}}{\hat{\xi}}, & \text{if } 0 \leq \hat{t} < \hat{\xi} \\ a, & \text{if } \hat{\xi} \leq \hat{t} < \hat{\tau} + \hat{\xi} \\ a\left(\frac{\hat{\tau}+2\hat{\xi}-\hat{t}}{\hat{\xi}}\right), & \text{if } \hat{\tau} + \hat{\xi} \leq \hat{t} < \hat{\tau} + 2\hat{\xi} \\ 0, & \text{if } \hat{t} \geq \hat{\tau} + 2\hat{\xi} \end{cases} \tag{3.6.29}$$

where $\hat{\xi}$ denotes the pulse rise or fall in time and $\hat{\tau}$ denotes the duration of the pulse as shown in figure (3.3). For convenience, let $\hat{v}^*_{\hat{\beta}}(\hat{x}, \hat{t})$ and $\hat{\mathcal{P}}^*_{\hat{\beta}}(\hat{t})$ be the dimensionless discharge velocity and dimensionless fluid power density respectively which result from the application of the dimensionless trapezoidal-pulse driving term $\hat{F}(\hat{t})$. On the application of Heaviside function

$H(\hat{t})$ defined in (3.6.18), then (3.6.29) can be expressed as follows:

$$\begin{aligned}\hat{F}(\hat{t}) =& 0\Big(H(\hat{t}-0)\Big) + \frac{a\hat{t}}{\hat{\xi}}\Big(H(\hat{t}-0) - H(\hat{t}-\hat{\xi})\Big) + a\Big(H(\hat{t}-\hat{\xi}) - H(\hat{t}-(\hat{\tau}+\hat{\xi}))\Big) \\ &+ a\Big(\frac{\hat{\tau}+2\hat{\xi}-\hat{t}}{\hat{\xi}}\Big)\Big(H(\hat{t}-(\hat{\tau}-\hat{\xi})) - H(\hat{t}-(\hat{\tau}+2\hat{\xi}))\Big) + 0\Big(H(\hat{t}-(\hat{\tau}+2\hat{\xi}))\Big) \\ \implies \hat{F}(\hat{t}) =& \frac{a}{\hat{\xi}}\Big(\hat{t}H(\hat{t}) - (\hat{t}-\hat{\xi})H(\hat{t}-\hat{\xi}) - (\hat{t}-\hat{\tau}-\hat{\xi})H(\hat{t}-\hat{\tau}-\hat{\xi}) - (\hat{t}-\hat{\tau}-2\hat{\xi})H(\hat{t}-\hat{\tau}-2\hat{\xi})\Big).\end{aligned} \tag{3.6.30}$$

Now to compute $\hat{v}^*_{\hat{\beta}}(\hat{x},\hat{t})$, first make the following observations: Using the expression in (3.6.19) yields

$$\int_0^{\hat{t}} \hat{u}_{\hat{\beta}}(\hat{x},s)ds = -2\sum_{n=1}^{\infty} \frac{(-1)^{n-1}y_n(\hat{x})}{1+\hat{\beta}\hat{\lambda}_n}\Big(\hat{t} - \frac{1+\hat{\beta}\hat{\lambda}_n}{\hat{\lambda}_n} + \frac{1+\hat{\beta}\hat{\lambda}_n}{\hat{\lambda}_n}\exp\Big(-\frac{\hat{\lambda}_n}{1+\hat{\beta}\hat{\lambda}_n}\hat{t}\Big)\Big), \tag{3.6.31}$$

and taking $\hat{F}(\hat{t}) = \hat{t}H(\hat{t})$, it follows from the expression in (3.6.15) that

$$\hat{u}(\hat{x},\hat{t}) = \int_0^{\hat{t}} \hat{u}_{\hat{\beta}}(\hat{x},s)ds, \tag{3.6.32}$$

so that using (3.6.32) it follows from (3.4.12) that

$$\hat{v}(\hat{x},\hat{t}) = -\frac{\partial \hat{u}(\hat{x},\hat{t})}{\partial \hat{t}} = -\hat{u}_{\hat{\beta}}(\hat{x},\hat{t}).$$

Hence, applying the linear superposition principle, $\hat{v}^*_{\hat{\beta}}(\hat{x},\hat{t})$ is the linear combination of the discharge velocities corresponding to the several components of the pulse, i.e.

$$\begin{aligned}\hat{v}^*_{\hat{\beta}}(\hat{x},\hat{t}) =& \frac{a}{\hat{\xi}}\Big(-\hat{u}_{\hat{\beta}}(\hat{x},\hat{t})H(\hat{t}) + \hat{u}_{\hat{\beta}}(\hat{x},\hat{t}-\hat{\xi})H(\hat{t}-\hat{\xi}) + \hat{u}_{\hat{\beta}}(\hat{x},\hat{t}-\hat{\tau}-\hat{\xi})H(\hat{t}-\hat{\tau}-\hat{\xi}) \\ &+ \hat{u}_{\hat{\beta}}(\hat{x},\hat{t}-\hat{\tau}-2\hat{\xi})H(\hat{t}-\hat{\tau}-2\hat{\xi})\Big).\end{aligned} \tag{3.6.33}$$

Using (3.4.24) and (3.6.33) the dimensionless power density $\hat{\mathcal{P}}^*_{\hat{\beta}}(\hat{t})$ is computed as

$$\hat{\mathcal{P}}^*_{\hat{\beta}}(\hat{t}) = \frac{a^2}{\hat{\xi}^2}\int_0^1 \Big(\hat{u}_{\hat{\beta}}(\hat{x},\hat{t})H(\hat{t}) - \hat{u}_{\hat{\beta}}(\hat{x},\hat{t}-\hat{\xi})H(\hat{t}-\hat{\xi}) - \hat{u}_{\hat{\beta}}(\hat{x},\hat{t}-\hat{\tau}-\hat{\xi})H(\hat{t}-\hat{\tau}-\hat{\xi}) \\ -\hat{u}_{\hat{\beta}}(\hat{x},\hat{t}-\hat{\tau}-2\hat{\xi})H(\hat{t}-\hat{\tau}-2\hat{\xi})\Big)^2 d\hat{x}. \tag{3.6.34}$$

If the amplitude $a = 1$, the maximum discharge velocity denoted by $\hat{v}^*_{\max}(\hat{\beta},\hat{\xi})$ is attained at $\hat{x} = 1$, and $\hat{t} = \hat{\xi}$, and is computed as:

$$\hat{v}^*_{\max}(\hat{\beta},\hat{\xi}) = \max_{\substack{0\le\hat{x}\le 1\\ \hat{t}\ge 0}} \hat{v}^*_{\hat{\beta}}(\hat{x},\hat{t}) = \hat{v}^*_{\hat{\beta}}(1,\hat{\xi}) \tag{3.6.35}$$

$$= \frac{2}{\hat{\xi}}\sum_{n=1}^{\infty}\frac{1}{\hat{\lambda}_n}\Big(1-\exp\Big(-\frac{\hat{\lambda}_n\hat{\xi}}{1+\hat{\lambda}_n\hat{\beta}}\Big)\Big), \tag{3.6.36}$$

and at $\hat{t} = \hat{\xi}$ the maximum dimensionless fluid power density, denoted by $\hat{\mathcal{P}}^*_{\max}(\hat{\beta},\hat{\xi})$ is attained and is computed as:

$$\hat{\mathcal{P}}^*_{\max}(\hat{\beta},\hat{\xi}) = \max_{t\ge 0}\hat{\mathcal{P}}^*_{\hat{\beta}}(\hat{t}) = \hat{\mathcal{P}}^*_{\hat{\beta}}(\hat{\xi}) \tag{3.6.37}$$

$$= \frac{4}{\hat{\xi}^2}\sum_{n=1}^{\infty}\left(\frac{1-\exp(-\frac{\hat{\lambda}_n\hat{\xi}}{1+\hat{\beta}\hat{\lambda}_n})}{\hat{\lambda}_n}\right)^2. \tag{3.6.38}$$

It is noted that for any $\hat{\beta} > 0$ and $\hat{\xi} > 0$,

$$\hat{v}^*_{\max}(\hat{\beta},\hat{\xi}) \le \lim_{\hat{\xi}\to 0}\hat{v}^*_{\max}(\hat{\beta},\hat{\xi}), \tag{3.6.39}$$

and

$$\lim_{\hat{\xi}\to 0}\hat{v}^*_{\max}(\hat{\beta},\hat{\xi}) = \hat{v}_{\max}(\hat{\beta}),$$

where $\hat{v}_{\max}(\hat{\beta})$ is given by (3.6.26). This is true since the trapezoidal pulse reduces to a rectan-

gular pulse as $\hat{\xi} \to 0$. Now for all $\hat{\beta} \geq 0$ and $\hat{\xi} > 0$,

$$\hat{v}^*_{\max}(\hat{\beta}, \hat{\xi}) \leq \hat{v}^*_{\max}(0, \hat{\xi}) = \frac{2}{\hat{\xi}} \sum_{n=1}^{\infty} \frac{1 - \exp(-\hat{\lambda}_n \hat{\xi})}{\hat{\lambda}_n}. \tag{3.6.40}$$

Next chapter presents the results and the discussions of the analysis presented in this chapter based on the dimensionless medium structural viscoelasticity when the boundary traction is either step-pulse or trapezoidal-pulse in time.

CHAPTER 4

RESULTS AND DISCUSSION

4.1 Results

This section provides the space-time behaviors of the dimensionless solid displacements $\hat{u}$, dimensionless fluid velocity $\hat{v}$, and dimensionless fluid power density $\hat{\mathcal{P}}$ when the porous medium is purely elastic $(\hat{\beta} = 0)$ and viscoelastic $(\hat{\beta} = 1)$ subject to different boundary tractions using MATLAB.

The MATLAB scripts in A.1, A.2 and A.3 are used to compute (3.6.19), (3.6.20) and (3.6.21) respectively for $\hat{\beta} = 0$, and $\hat{\beta} = 1$, in order to produce the space-time behaviour of $\hat{u}_{\hat{\beta}},\ \hat{v}_{\hat{\beta}}$, and $\hat{\mathcal{P}}_{\hat{\beta}}$ in Figures $4.1, 4.2$ and 4.3 respectively.

The MATLAB script in A.4 is used to compute (3.6.24) for $\hat{\beta} \in [0, 1]$ and the result of this computation is given in Figure 4.4.

The MATLAB scripts in A.5 is used in the numerical computations of (3.6.26) and (3.6.27) respectively to give Figure 4.5.

Figure 4.6 is as a result of the computation of (3.6.28) by setting $\frac{K_0}{L} = 1$, and $F_{spec} \in [10^{-4}, 10^{4}]\text{Nm}^{-2}$ using the MATLAB scripts in A.6. The arrows in both diagrams of Figure 4.6 indicate increase in F_{spec}.

For $\hat{\beta} \geq 0,\ a = 1, \hat{\xi} > 0$, and $\hat{\tau} = 1$, a typical space time behaviour of the dimensionless discharge velocity $\hat{v}^*_{\hat{\beta}}(\hat{x}, \hat{t})$ and dimensionless fluid power density $\hat{\mathcal{P}}^*_{\hat{\beta}}(\hat{t})$ are produced in Figures 4.7 and 4.8 respectively using the MATLAB scripts in A.7 and A.8. The dimensionless maximum discharge velocity in (3.6.35) is computed using the MATLAB script in A.9 to show the behaviour of $\hat{v}^*_{\max}$ with respect to $\hat{\beta}$ and $\hat{\xi}$ as given in Figure 4.9.

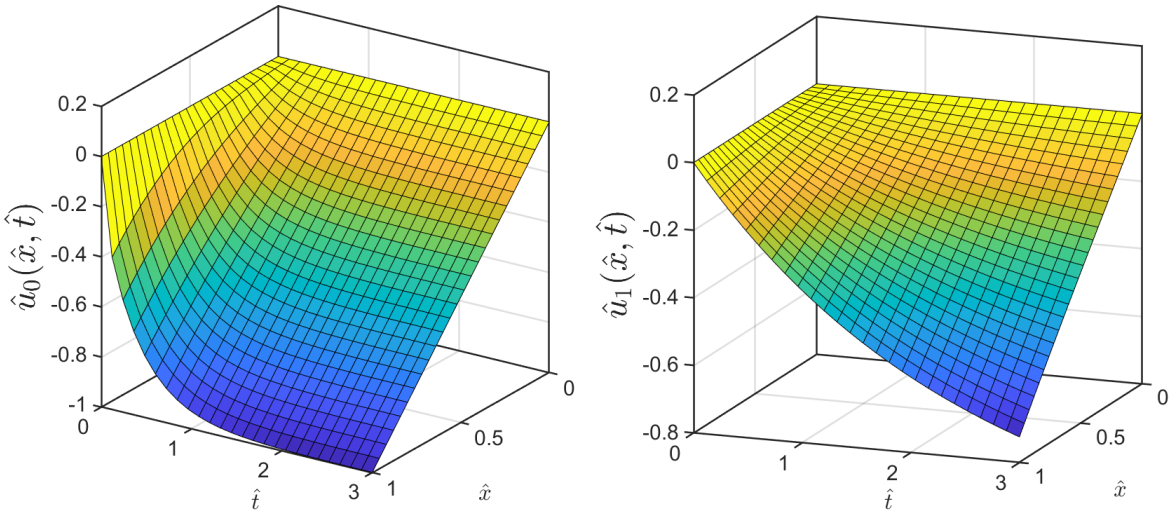

Figure 4.1. Dimensionless displacement as a function of $\hat{x}$, and $\hat{t}$. Left diagram: $\hat{\beta} = 0$. Right diagram: $\hat{\beta} = 1$

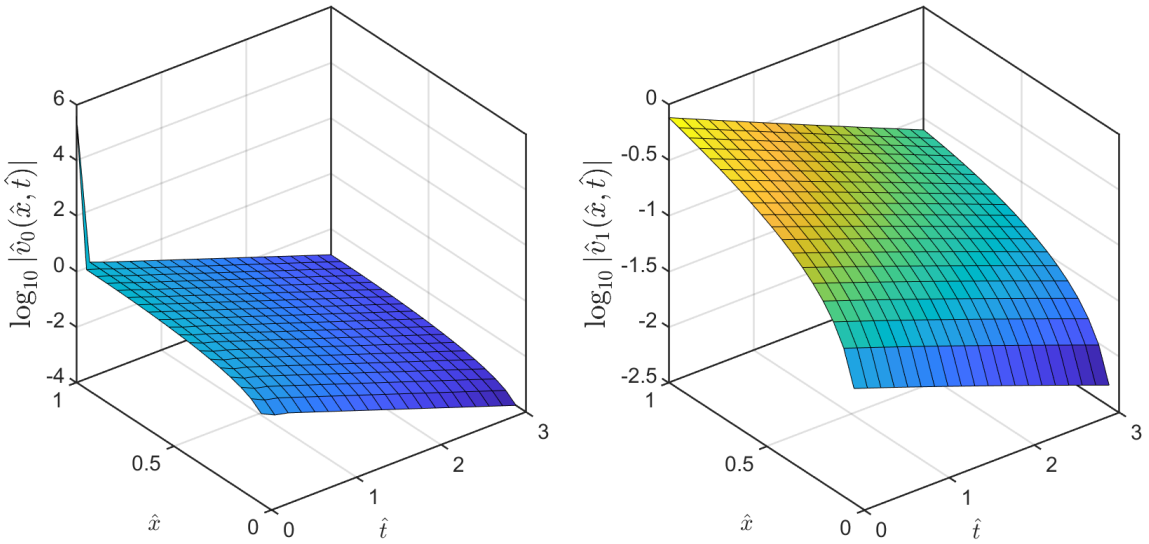

Figure 4.2. Dimensionless discharge velocity $\hat{v}_{\hat{\beta}}$ as a function of $\hat{x}$, and $\hat{t}$. Left diagram: $\hat{\beta} = 0$. Right diagram: $\hat{\beta} = 1$

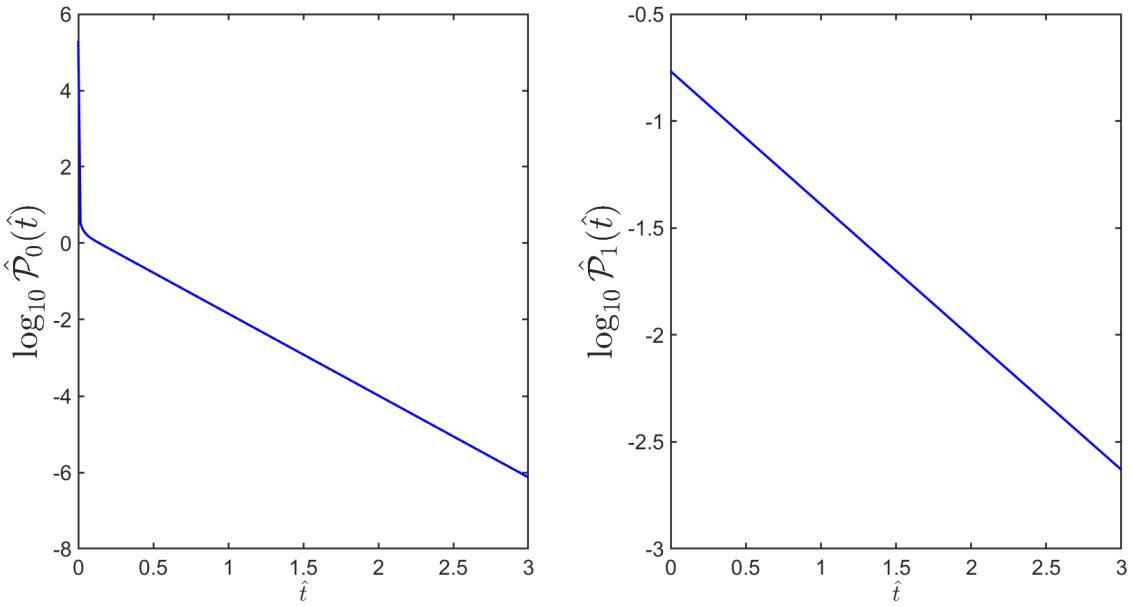

Figure 4.3. Dimensionless fluid power density $\hat{\mathcal{P}}_{\hat{\beta}}$ as a function $\hat{t}$: Left diagram: $\hat{\beta} = 0$. Right diagram: $\hat{\beta} = 1$

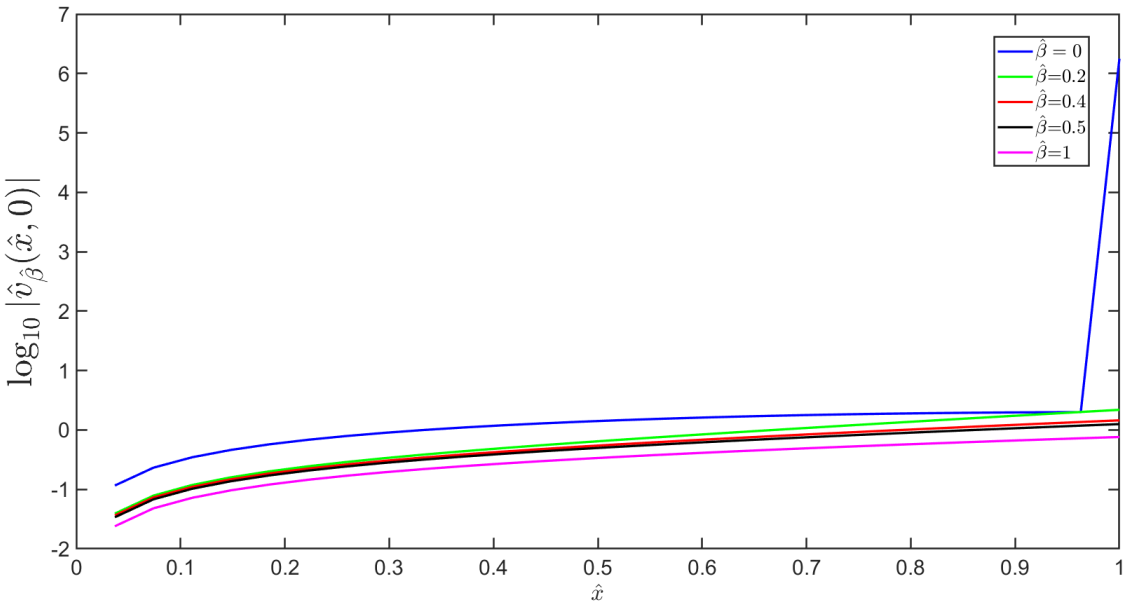

Figure 4.4. Dimensionless discharge velocity $\hat{v}_{\hat{\beta}}(\hat{x}, 0)$ as a function of $\hat{x}$ to highlight the velocity blow-up at $\hat{x} = 1$ when $\hat{\beta} = 0$.

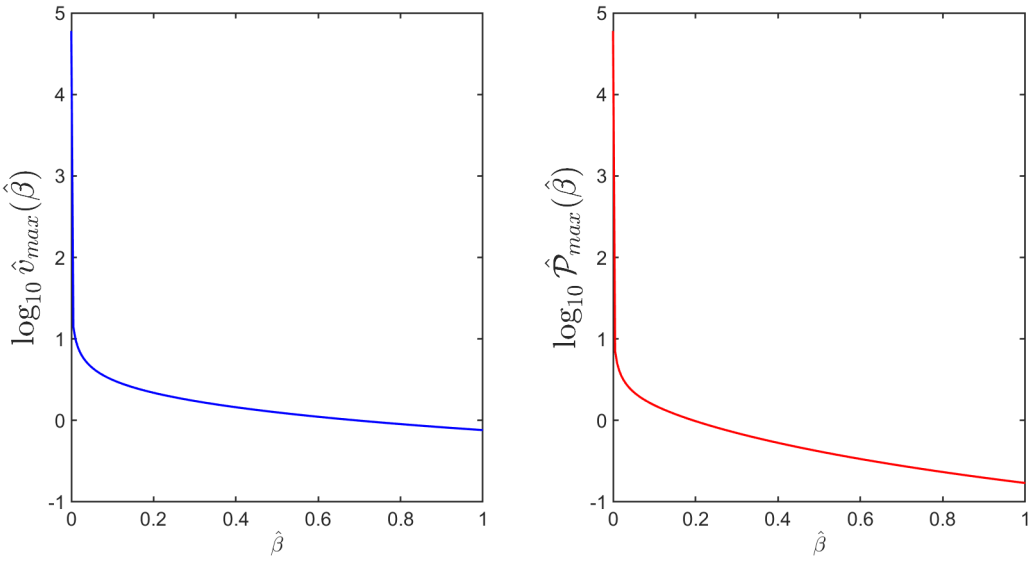

Figure 4.5. Left diagram: maximum discharge velocity as a function of $\hat{\beta}$. Right diagram: maximum power density as a function of $\hat{\beta}$.

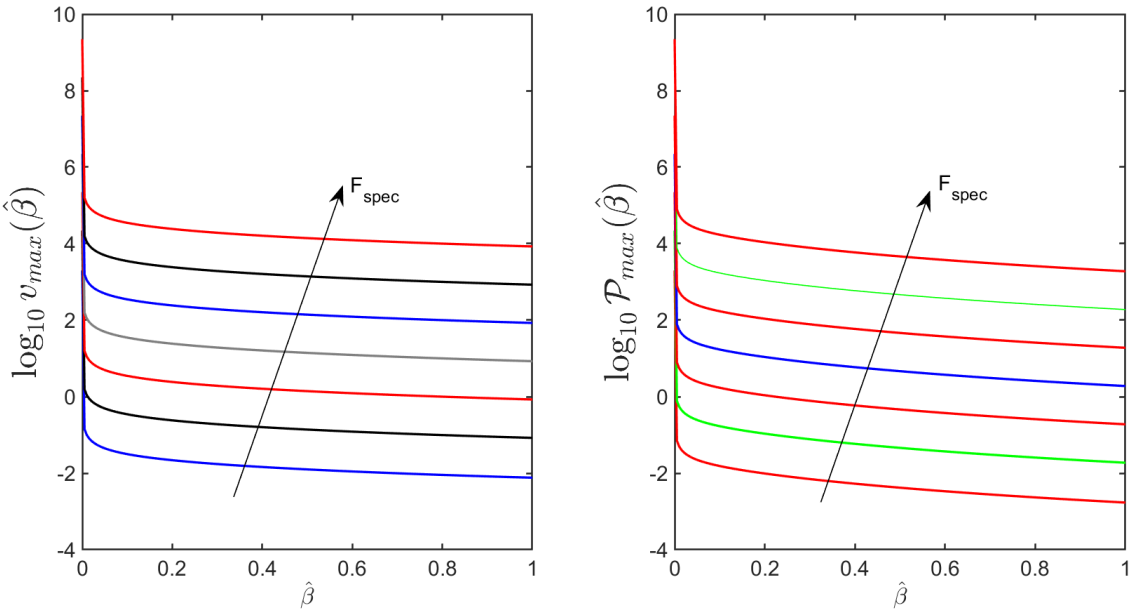

Figure 4.6. Left diagram: Dimensionless maximum discharge velocity as a function of $\hat{\beta}$. Right diagram: Dimensionless maximum power density as a function of $\hat{\beta}$.

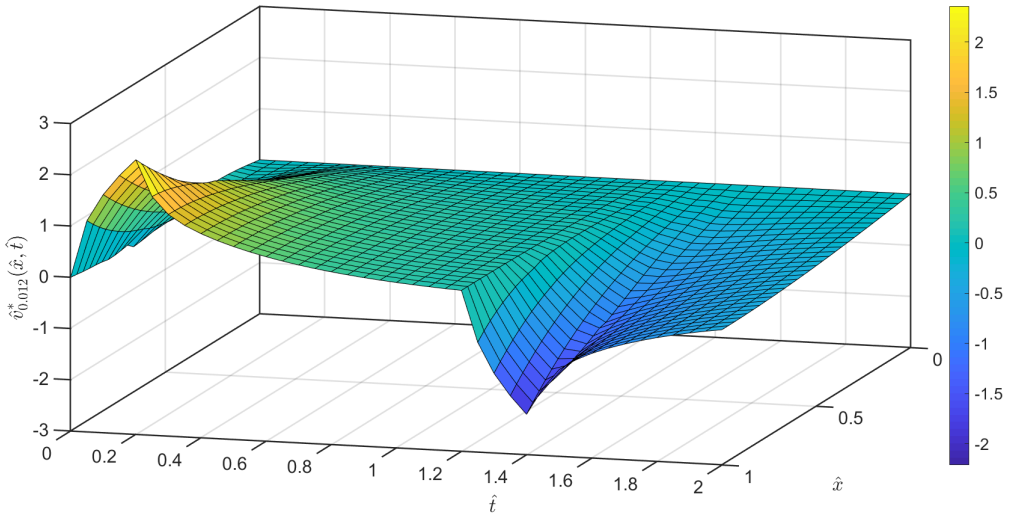

Figure 4.7. Dimensionless discharge velocity, $\hat{v}^*_{\hat{\beta}}(\hat{x},\hat{t})$ for $\hat{\beta} = 0.012,\ \hat{\xi} = 0.21,\ a = 1$ and $\hat{\tau} = 1$

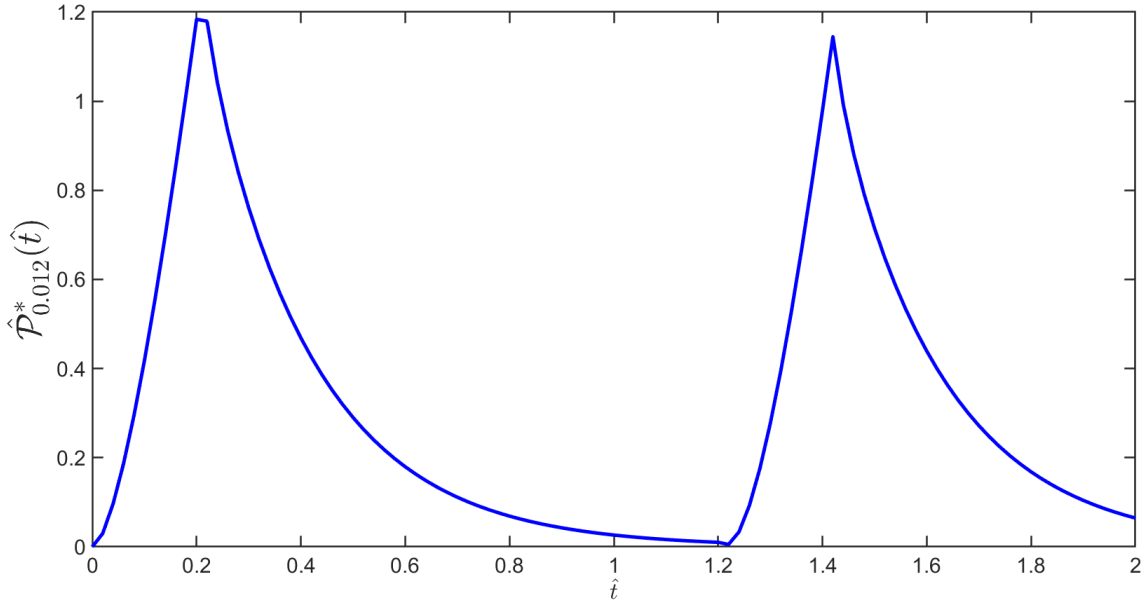

Figure 4.8. Dimensionless fluid power density, $\hat{\mathcal{P}}^*_{\hat{\beta}}(\hat{t})$ for $\hat{\beta} = 0.012,\ \hat{\xi} = 0.21,\ a = 1$ and $\hat{\tau} = 1$

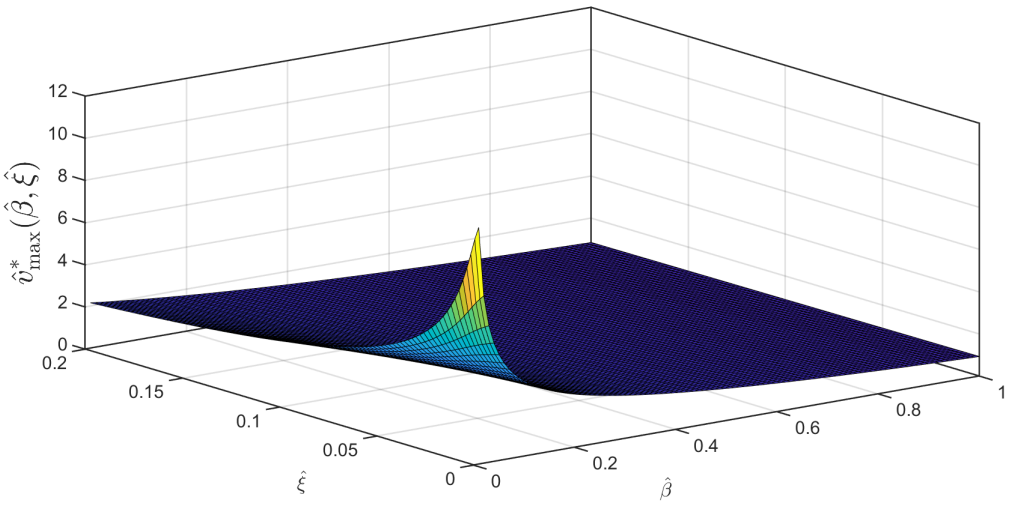

Figure 4.9. Dimensionless discharge velocity $\hat{v}^*_{\max}$ as a function of dimensionless pulse rise or fall in time $\hat{\xi}$ and dimensionless viscoelasticity $\hat{\beta}$.

4.2 Discussion

The goals of this study were to use the theory of poro-viscoelasticity to construct a one-dimensional mathematical model that clarifies the effect of structural viscoelasticity in the mechanical response of non-divergence free deformable porous medium when subjected to quasi-static time-dependent loading and unloading protocols, and then use the analysis to explain the confined compression experiment in biomechanics. With respect to the first objective, we found that the mathematical model involves a system of non-linear PDEs with boundary and initial conditions corresponding to that of creep experimental test utilized in CCE (Figure (3.1)). Following the study by (Banks et al., 2017; Lorena et al., 2016), the system of PDEs was linearized by assuming a constant medium permeability. Also, the assumption of infinitesimal deformation of the porous medium makes it possible for the solid displacement and fluid velocity not to be divergent free even though the medium constituents are incompressible.

The second objective of this study was to obtain an explicit solution for the mathematical model in one-dimension. Here, it was found that if the boundary forcing term (traction force) $F(t)$, belongs to the space of strongly measurable functions $\mathcal{L}^2(0,T)$ then there exists a unique weak solution $u(x,t)$ to the model in a well-defined functional space, and by using the stronger assumption that $F(t) \in \mathcal{L}^\infty(0,T)$ the derivative of the solution with respect to time converges absolutely and uniformly in $[0,L] \times [0,T]$ and hence continuous. Dimensional

analysis was engaged to demonstrate the physical and geometrical quantities that can influence solution properties when the external applied load is characterised by a step or a trapezoidal pulse. The explicit formula initially obtained enabled us to go about the choice of characteristic values for the purpose of scaling physical quantities. Knowing that the system is driven by boundary source of traction, so our interest is to access the influence of an external load on the mechanical response of the medium and as such, the characteristic velocity utilized is the one induced by the external load of magnitude F_{spec}. The third objective of this study was to demonstrate that the sole determinant of the alteration in the fluid-mechanics within the porous medium is the viscoelastic parameter, $\hat{\beta}$ under different boundary tractions $\hat{F}(\hat{t})$.

When $\hat{F}(\hat{t})$ is the unit step-pulse in (3.6.18) the following were observed: Figure 4.1 shows that the particles of the porous material are significantly displaced in the purely elastic case $(\hat{\beta} = 0)$ than when viscoelasticity is present $(\hat{\beta} = 1)$. First, from the scaling in (3.6.1) it can be seen that

$$\hat{\beta} = 0 \implies \hat{\beta} = \frac{\beta}{[\beta]} = 0 \tag{4.2.1}$$

From (4.2.1),

$$\beta = 0,\ [\beta] \neq 0, \quad \text{or} \quad [\beta] \to \infty \ \left(\text{where } [\beta] = \frac{L^2}{K_0}\right). \tag{4.2.2}$$

When $\beta = 0$, then it means that either the medium stiffness due to viscoelasticity is zero, and/or no viscoelastic effect due to the medium ((3.4.5)), and hence leads to $\hat{\beta} = 0$. When $[\beta] \to \infty$ (approaching a very large value), then it follows from the scaling for $[\beta]$ in (3.6.4) that the medium permeability is too small (of order 10^{-10}) or even negligible provided the medium thickness (in this study $L = 1m$), and β be fixed respectively could result to the condition in (4.2.1). Subjecting the porous medium with any of these conditions to a time-discontinuous loading system explains the reason for the sharp change in the solid displacement when $\hat{\beta} = 0$ as shown in Figure 4.1.

In Figure 4.2, the fluid velocity $\hat{v}_{\hat{\beta}}$ tends to infinity (this is called velocity blow-up) in the purely elastic case $\hat{\beta} = 0$ than in the viscoelastic case $\hat{\beta} = 1$. From physical view points, this can be interpreted as: at the start of time, $\hat{t} = 0$, of the load, the discharge velocity has high-frequency

components whose superposition displays the following behaviours:

i) It approaches infinity as $\hat{x}$ approaches 1, and hence leading to its blow-up

ii) It relaxes towards zero as $\hat{x}$ approaches 0

iii) It has an amorphous structure for $0 < \hat{x} < 1$.

Figure 4.3 shows that the dimensionless fluid power density tends to infinity (power density blow-up) in the purely elastic medium (i.e. $\hat{\beta} = 0$) but remains bounded when the medium is viscoelastic (i.e. $\hat{\beta} = 1$). Further illustration of the blow-up in dimensionless discharge velocity is presented in Figure (4.4) at $\hat{t} = 0$ for values of $\hat{\beta} \in [0, 1]$ (Note that the spatial distribution of $\hat{v}_{\hat{\beta}}(\hat{x}, \hat{t})$ is given in logarithmic scale to clearly see the blow-up), and this shows that the maximum value of dimensionless discharge velocity is attained near the surface of the porous medium which is in contact with the load (at $\hat{x} = 1$) when viscoelasticity is absent at time $\hat{t} = 0$. Table (4.1) gives the approximated maximum values of fluid discharge velocity and fluid power density for different values of $\hat{\beta}$ respectively.
The maximum value of power density is attained at the start of the load when $\hat{\beta} = 0$ (Figure 4.3). Figure 4.5 shows the sole determinant of the blow-up in dimensionless maximum fluid velocity and dimensionless power density respectively as the medium structural viscoelasticity $\hat{\beta}$. Figure (4.6) shows that increasing the magnitude, F_{spec} of the applied quasi-static load would result to velocity blow-up (maximum value spiking to infinity), and hence leads to fluid power density blow-up within the deformable porous medium.

When $\hat{F}(\hat{t})$ is the trapezoidal-pulse (continuous in time) in (3.6.29), it was found that both discharge velocity and power density remained bounded for $\hat{\xi} > 0$, and no blow-up occurred in both purely elastic and viscoelastic cases as shown in Figures 4.7, and 4.8 respectively. Figure 4.9 respectively. Figure 4.9 shows that the dimensionless maximum fluid velocity attained within the medium remains also bounded in both purely elastic ($\hat{\beta} = 0$) and viscoelastic ($\hat{\beta} = 1$) cases.

The next section validates the results of this study by using the mathematical analysis developed to study some important features of confined compression experiment of biomaterials (biological tissues) in order to provide directions on how to select structural properties for their

Value of $\hat{\beta}$	**value of $\hat{v}_{\hat{\beta}}(\hat{x},\hat{t})$ in m/s at $\hat{x}=1$**	**value of $\hat{\mathcal{P}}_{\hat{\beta}}(\hat{t})$ in $Jm^{-3}s^{-1}$ at $\hat{t}=0$**
0	$\approx 10^{7}$	$\approx 10^{7}$
0.0001	$\approx 10^{2}$	$\approx 10^{2}$
0.001	$\approx 10^{1.5}$	$\approx 10^{1.5}$
0.01	≈ 10	≈ 10
0.1	$\approx \sqrt{10}$	$\approx \sqrt{10}$
1	$\approx 10^{-0.8}$	$\approx 10^{-0.8}$

Table 4.1. Maximum values of dimensionless fluid velocity and power density attained for different values of $\hat{\beta}$ when the load profile is a step pulse

designs, and thus preventing them from microstructural damages which may result from fluid discharge velocity spiking to infinity.

4.3 Validation of Results

In the previous sections, it was found that fluid discharge velocity could tend to infinity should viscoelasticity be absent when the load profile experience sharp changes in time. This section uses this concept to study some interesting features of confined compression tests, which are often utilized in biomechanics to characterize the properties of biological tissues and hence aid their designs.

A schematic of the confined compression experimental setting is given in Figure 4.10, where a compressive load is applied at the top of the chamber while the bottom and the sides are fixed. The one-dimensional model considered in the previous Chapter 3 enables us to generalize the mathematical analysis carried out in (Soltz & Ateshian, 1998; Verri et al., 2017), by quantifying the effect of structural viscoelasticity on the tissue response to sudden changes in external pressure during CCE. Here;

i) L represents the thickness of the undeformed biological tissue sample.

ii) F_{spec} represents the magnitude of the total compressive stress force applied at $x = L$.

It is important to note that a typical confined compression creep experiment is characterized by the initial and boundary conditions in (3.4.8) to (3.4.10) Soltz & Ateshian (1998); Verri et al. (2017). However, the mathematical description utilized in (Banks et al., 2017) doesn't account for structural viscoelasticity, thus leads to setting $\beta = 0$ in (3.4.5). Table (4.2) summarizes

the parameter values obtained for the CCE on articular cartilage in (Banks et al., 2017). The characteristic velocities reported in (Banks et al., 2017) is of order $0.35 \times 10^{-6} m/s$. But the analysis in this study showed that velocities in the sample may attain much higher values, especially near the permeable pistol should viscoelasticity be low and/or the time profile of the compressive load be too sharp (see the left diagrams in figures (4.2), (4.4) and (4.5)). In other to make this concept more specific, assume that

i) the load protocol for the CCE corresponds to the trapezoidal pulse described in chapter 3, and

ii) the discharge velocities always remain below the threshold value $v_{th}^* = 0.35 \times 10^{-6} m/s$, so as to prevent the sample from microstructural damage. Using (3.6.1), (3.6.5) and values in the table (4.2) the dimensionless threshold velocity becomes

$$\hat{v}_{th}^* = \frac{L}{F_{spec} K_0} V_{th}^* = \frac{0.81 \times 10^{-3} \times 0.33 \times 10^{-6}}{6 \times 10^4 \times 2.9 \times 10^{-16}} = 16.3. \tag{4.3.1}$$

This means that $\hat{\beta}$ and $\hat{\xi}$ must be chosen in such a way that

$$\hat{v}_{\max}^*(\hat{\beta}, \hat{\xi}) < \hat{v}_{th}^* = 16.3.$$

Figure 4.11 compares $\hat{v}_{th}^*$ with the values of $\hat{v}_{\max}^*$ for different values of $\hat{\beta}$ and $\hat{\xi}$. In fact, a whole region in the $(\hat{\beta}, \hat{\xi})-$plane for which $\hat{v}_{\max}^*(\hat{\beta}, \hat{\xi}) < \hat{v}_{th}^*$ can be identified. To better see the various regions of interest in the $(\hat{\beta}, \hat{\xi})-$plane, the colormap of the difference $\hat{v}_{th}^* - \hat{v}_{\max}$ as a function of $\hat{\beta}$ and $\hat{\xi}$ is reported in Figure(4.12). Here, the region in the parameter space where $\hat{v}_{th}^* = \hat{v}_{\max}$ is clearly marked by the thick curve. These results show that, for example, choosing $\hat{\xi} \geq 5 \times 10^{-3}$ would lead to fluid velocities below the given threshold regardless of the presence of structural viscoelasticity. Should the particular experimental conditions restricts us to utilize a rectangular pulse corresponding to $\hat{\xi} = 0$, the maximum discharge velocity can still be maintained below the threshold by modifying the structural properties of the sample to have for example $\hat{\beta} \geq 4 \times 10^{-3}$ as shown in Figure 4.12.

From (3.6.1) and (3.6.4), it is seen that $\hat{\beta}$ can be increased by increasing the viscoelastic parameter β, increasing the medium permeability K_0, and/or decreasing the sample thickness

L. Following the work in (Čanić et al., 2006; Verri et al., 2017), a typical value of the viscoelastic parameter β, for biological tissues can be computed using

$$\beta = \alpha\tau_e, \tag{4.3.2}$$

where $\tau_e = L\sqrt{\frac{\rho}{\alpha}}$ is the characteristic elastic time constant of the porous material(biological tissue) under compression and ρ is the mass density of the fluid components. Since the densities of most of the interstitial biological fluids are similar to that of water, then take $\rho = 1000kg/m^3$. Substituting (4.3.2) into the scaling for $\hat{\beta}$ in (3.6.1) and (3.6.4) yields

$$\hat{\beta} = \frac{L^2\tau_e}{K_0[t][\beta]} = \frac{K_0}{L}\sqrt{\rho\alpha}, \tag{4.3.3}$$

so that using the parameter values in table (4.2) gives

$$\hat{\beta} = 1.15 \times 10^{-8}.$$

This value is 5 order of magnitude smaller than what is required to attain fluid discharge velocities below the recommended threshold in the situation of a rectangular pulse in the pressure load. Hence, in order to control the maximum fluid discharge velocity within the porous material, it is important to

i) vary the properties of the tissue sample by manipulating ρ, α, β, K_0 or L and

ii) vary the time profile of the load experimental protocol.

All these will depend on the specific conditions and restriction of the experiment under consideration.

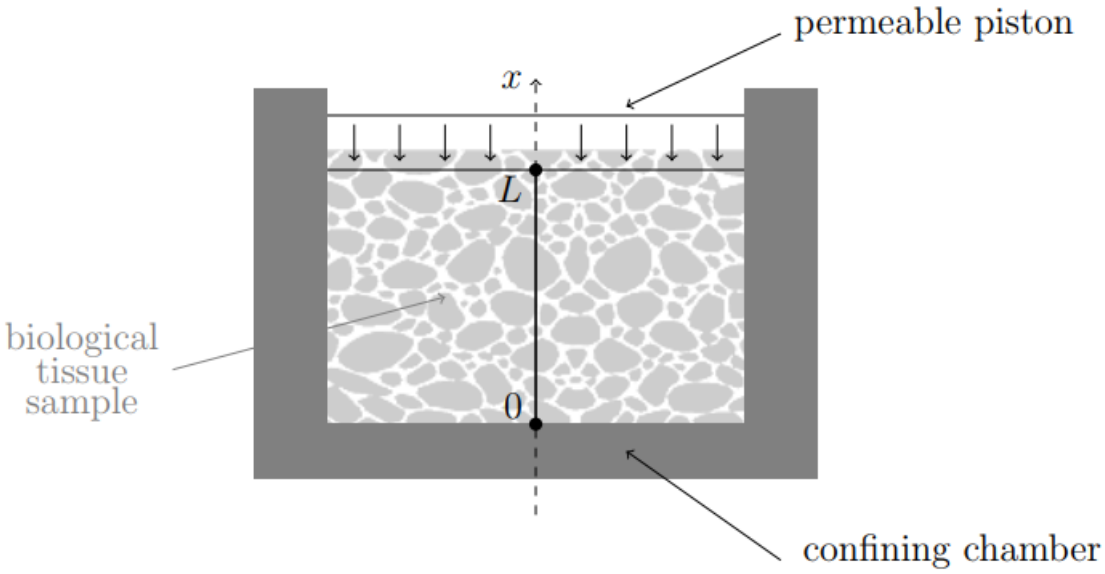

Figure 4.10. Schematic of confined compression test of biological tissue

.

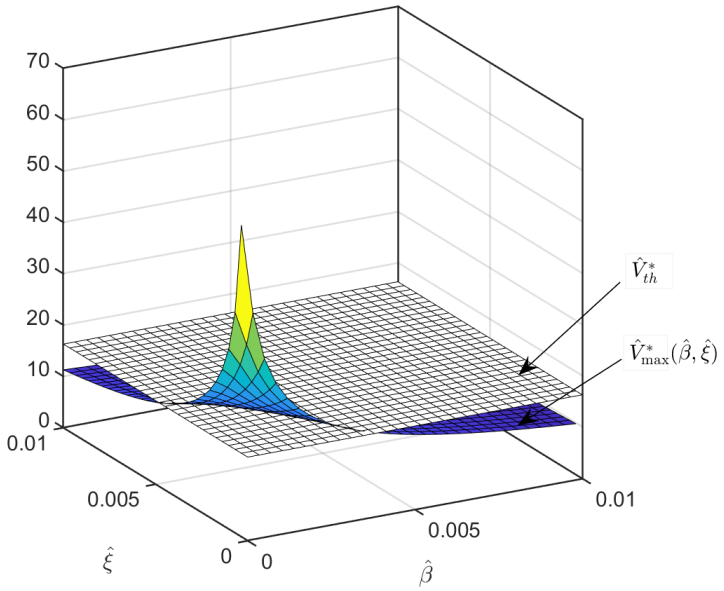

Figure 4.11. Comparison between $\hat{v}^*_{\max}(\hat{\beta},\hat{\xi})$ obtained using expression(3.6.35) and the dimensionless threshold velocity $\hat{v}^*_{th} = 16.3$ typical of confined compression experiments.

.

Symbol	Numerical value
α	$0.81 \times 10^{-3} Nm^{-2}$
β	$0 Nm^{-2}$
L	$0.81 \times 10^{-3} m$
K_0	$2.9 \times 10^{-16} N^{-1} m^4 s^{-1}$
F_{spec}	$6 \times 10^4 Nm^{-2}$

Table 4.2. Numerical values of model parameters in the confined compression experiments for articular cartilage (Verri et al., 2017)

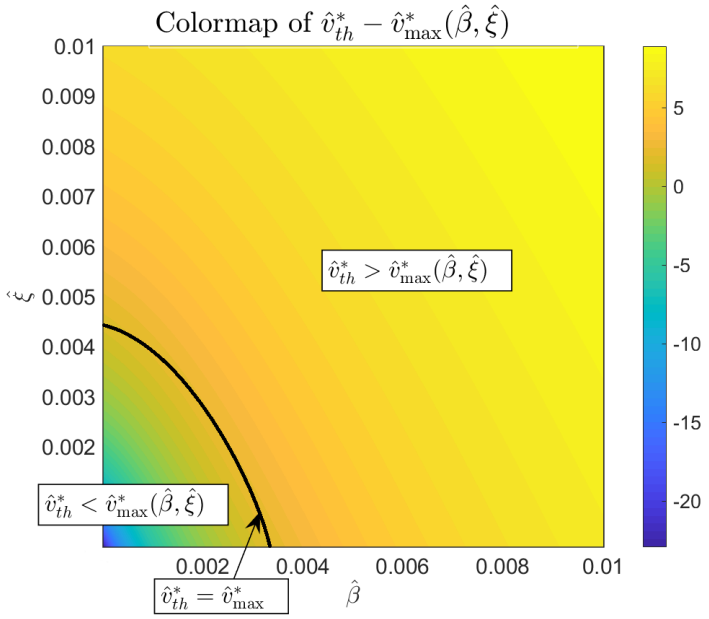

Figure 4.12. Colormap of $\hat{v}^*_{th} - \hat{v}^*_{\max}$ in the $(\hat{\beta}, \hat{\xi})-$plane. $\hat{v}^*_{max}$ is obtained by (3.6.35) and $\hat{v}^*_{th} = 16.3$. The thick curve indicates points where $\hat{v}^*_{th} = \hat{v}^*_{\max}$.

.

The strengths and weaknesses of the present study are discussed in the next section.

4.4 Strengths and Weaknesses

Most of the available literatures studied poro-elasticity with no account for medium structural viscoelasticity. The present study has been able to use the theory of poro-viscoelasticity, a coupling between structural viscoelasticity and poro-elasticity, to study the effect of structural viscoelasticity in the mechanical response of deformable porous medium with incompressible constituents to quasi-static loading system, and provided series of conditions that could cause the fluid velocity, and hence power density blow-ups within the porous medium. The mathematical analysis developed is a generalization of the confined compression experiment used in

biomechanics for biomaterial designs. These are the major strengths of this study.

The present study didn't account for a deformable porous medium with compressible constituents, and so for situations utilizing this type of medium need to consider expression (3.3.6) rather than (3.3.8) for the increment of fluid content. Furthermore, the study was based on porous media which undergoes infinitesimal (small) strain (quantified by the strain tensor in (3.3.10)) under applied stress. So the settings involving large deformation need to replace this expression by the appropriate tensor.

Finally, the formulation for the mathematical model considered in this thesis assumed that the medium is not influenced by inertia ((3.3.4)).

CHAPTER 5

CONCLUSION AND RECOMMENDATION

5.1 Conclusion

In this study, the theory of poro-viscoelasticity has been utilized to access the effect of structural viscoelasticity in the mechanical response of non divergence-free deformable porous medium with incompressible constituents under quasi-static loading conditions in one-dimension. To the mathematical model, obtained an analytic solution which through dimensional analysis enabled us to identify main factors that cause fluid velocity blow-up within the deformable porous medium, namely the absence of structural viscoelasticity and time-discontinuity of the boundary forcing term. It was found that even a small presence of medium viscoelasticity prevented the blow-up. Also, when the boundary source of traction was continuous in time prevented the blow-up even in the purely elastic case (no viscoelasticity). The one-dimensional model considered in this study show that it is not possible to bound the fluid power density when the structure is purely elastic and the boundary source of traction has time discontinuity.

In reality, we will never see the fluid velocity tending to infinity as shown by the mathematical analysis in this thesis because something will break first, for instance, if the poro-viscoelastic model represents a biological tissue containing capillaries through which blood flows, as the maximum fluid velocity becomes very high, the capillaries will break and let out blood. Hence, from the practical point of view, it is important to identify parameters that can control the maximum values of the fluid velocity within the deformable porous medium so as to avoid microstructural damages. This study found that the maximum values of fluid velocity within the porous medium can be maintained below a normal threshold by:

i) decreasing the magnitude of the load F_{spec}, and thus reducing the load on the medium,

ii) increasing the pulse rise and fall $\hat{\xi}$, and hence smoothing the applied load,

iii) decreasing the medium permeability K_0, and thus changing the pore size, medium geometry and/or fluid viscosity within the medium

- decreasing the thickness L, of the porous medium, and thus changing the domain geometry

iv) increasing structural viscoelasticity β, and hence changing the structural property of the solid component of the medium.

These concepts were further investigated in details by utilizing them in the confined compression experiments for biological tissues.

Furthermore, the mathematical analysis provided in this study complies with the conclusions in (Sack et al., 2009) where experimental data based on magnetic resonance elastography showed that structural viscoelasticity of the brain is a result of structural alteration occurring in the course of physiological aging, and as such, cerebral viscoelasticity may provide a sensitive identifier for a variety of neurological diseases such as Alzheimer's disease, Multiple sclerosis(Verri et al., 2017).

5.2 Recommendations

For future research, the mathematical analysis developed in this study can be extended for a wider application in the following ways:

i) by considering a deformable porous medium with compressible constituents, and as such the expression in (3.3.6) will be utilized instead of (3.3.8). This is of interest in the wider context of applications of the poro-viscoelastic model to problems in geomechanics.

ii) situations where there is large deformation in the porous medium can be investigated, and this case mathematically corresponds to considering the lagrange strain tensor (Lai et al., 2009) instead of the infinitesimal strain tensor in (3.3.10).

iii) time-discontinuities in the volumetric sources of linear momentum which was pointed out by (Lorena et al., 2016) as addition causes of blow-up can be investigated. This case

is relevant in situations where there is abrupt variation in the acceleration due to gravity, such as the one in space flight take off and landing.

REFERENCES

Athanasiou, K. A. & Natoli, R. M. (2008). Introduction to continuum biomechanics. *Synthesis lectures on biomedical engineering*, *3*(1), 1–206.

Augat, P. & Schorlemmer, S. (2006). The role of cortical bone and its microstructure in bone strength. *Age and ageing*, *35*(suppl_2), ii27–ii31.

Banks, H., Bekele-Maxwell, K., Bociu, L., Noorman, M., & Guidoboni, G. (2017). Sensitivity analysis in poro-elastic and poro-visco-elastic models with respect to boundary data. *Quarterly of Applied Mathematics*, *75*(4), 697–735.

Biot, M. A. (1941). General theory of three-dimensional consolidation. *Journal of applied physics*, *12*(2), 155–164.

Bowers, A. & Kalton, N. J. (2014). *An introductory course in functional analysis*. Springer.

Brezis, H. (2010). *Functional analysis, Sobolev spaces and partial differential equations*. Springer Science & Business Media.

Čanić, S., Tambača, J., Guidoboni, G., Mikelić, A., Hartley, C. J., & Rosenstrauch, D. (2006). Modeling viscoelastic behavior of arterial walls and their interaction with pulsatile blood flow. *SIAM Journal on Applied Mathematics*, *67*(1), 164–193.

Cao, R., Cheng, L., & Lian, P. (2015). Flow behavior of viscoelastic polymer solution in porous media. *Journal of Dispersion Science and Technology*, *36*(1), 41–50.

Cao, Y., Chen, S., & Meir, A. (2013). Analysis and numerical approximations of equations of nonlinear poroelasticity. *Discrete & Continuous Dynamical Systems-Series B*, *18*(5).

Cheng, A. H.-D. (2016). *Poroelasticity*, volume 27. Springer.

Coussy, O. (2004). *Poromechanics*. John Wiley & Sons.

De, S., Das, S., Kuipers, J. A. M., Peters, E. A. J. F., & Padding, J. T. (2016). A coupled finite volume immersed boundary method for simulating 3d viscoelastic flows in complex geometries. *Journal of Non-Newtonian Fluid Mechanics,*, 232, 67–76.

De, S., Kuipers, J. A. M., Peters, E. A. J. F., & Padding, J. T. (2017). Viscoelastic flow simulations in model porous media. *Physical Review Fluids*, 2(5), 053303.

Dominique, C., Gerbeau, J.-F., Sainte-Marie, J., & Clementel., I. E. V. (2010). A poroelastic model valid in large strains with applications to perfusion in cardiac modeling. *Computational Mechanics*, 46(1), 91–101.

Downs, J. C., Suh, J. F., Thomas, K. A., Bellezza, A. J., Hart, R. T., & Burgoyne, C. F. (2005). Viscoelastic material properties of the peripapillary sclera in normal and early-glaucoma monkey eyes. *Investigative ophthalmology & visual science*, *46*(2), 540–546.

Erdman, J. M. (2018). *A Problems Based Course in Advanced Calculus*, volume 32. American Mathematical Society.

Ghabezloo, S., Sulem, J., & Saint-Marc, J. (2009). Evaluation of a permeability–porosity relationship in a low-permeability creeping material using a single transient test. *International Journal of Rock Mechanics and Mining Sciences*, *46*(4), 761–768.

Haroske, D. & Triebel, H. (2008). *Distributions, Sobolev spaces, elliptic equations*, volume 5. European Mathematical Society.

Holzapfel, G. A. & Ogden, R. W. (2017). *Biomechanics: Trends in Modeling and Simulation*, volume 316. Springer.

Hutter, K., Wang, Y., et al. (2016). *Fluid and thermodynamics*. Springer.

Jacobs, N. T., Cortes, D. H., Peloquin, J. M., Vresilovic, E. J., & Elliott, D. M. (2014). Validation and application of an intervertebral disc finite element model utilizing independently constructed tissue-level constitutive formulations that are nonlinear, anisotropic, and time-dependent. *Journal of biomechanics*, 47(11), 2540–2546.

Jansen, J. D. (2013). *A systems description of flow through porous media*, volume 570. Springer.

Jeanne, P., Guglielmi, Y., Rutqvist, J., Nussbaum, C., & Birkholzer, J. (2018). Permeability variations associated with fault reactivation in a claystone formation investigated by field experiments and numerical simulations. *Journal of Geophysical Research: Solid Earth*, *123*(2), 1694–1710.

Keener, J. P. (2018). *Principles of applied mathematics : transformation and approximation*. CRC Press.

Khanafer, K., AlAmiri, A., Pop, I., & Bull, J. L. (2008). *Flow and heat transfer in biological tissues: application of porous media theory*. Springer.

Kim, M. (2017). Viscoelastic fluid flow through porous media modeled using pillared microchannels.

Lai, W. M., Hou, J. S., & Mow, V. C. (1991). A triphasic theory for the swelling and deformation behaviors of articular cartilage. *Journal of Biomechanical Engineering*, 113(3), 245–258.

Lai, W. M., Rubin, D. H., Krempl, E., & Rubin, D. (2009). *Introduction to continuum mechanics*. Butterworth-Heinemann.

London, G. M., Marchais, S. J., Guerin, A. P., Metivier, F., & Adda, H. (2002). Arterial structure and function in end-stage renal disease. *Nephrology Dialysis Transplantation*, *17*(10), 1713–1724.

Lorena, B., Guidoboni, G., Sacco, R., & Webster, J. T. (2016). Analysis of nonlinear poro-elastic and poro-visco-elastic models. *Archive for Rational Mechanics and Analysis*, 222(3),1445–1519.

Loret, B. & Huyghe, J. M. (2014). *Chemo-mechanical couplings in porous media geomechanics and biomechanics*, volume 462. Springer.

Lu, X. L. & Mow, V. C. (2008). Biomechanics of articular cartilage and determination of material properties. *Medicine & Science in Sports & Exercise*, *40*(2), 193–199.

Maccabi, A., Shin, A., Namiri, N. K., Bajwa, N., John, M. S., Taylor, Z. D., Grundfest, W., & Saddik, G. N. (2018). Quantitative characterization of viscoelastic behavior in tissue-mimicking phantoms and ex vivo animal tissues. *PloS one*, *13*(1), e0191919.

Marin, M. & Öchsner, A. (2018). *Essentials of Partial Differential Equations: With Applications*. Springer.

Moore, A., Zimmerman, B., Chen, X., Lu, X., & Burris, D. (2015). Experimental characterization of biphasic materials using rate-controlled hertzian indentation. *Tribology international*, *89*, 2–8.

Nia, H. T., Han, L., Li, Y., Ortiz, C., & Grodzinsky, A. (2011). Poroelasticity of cartilage at the nanoscale. *Biophysical journal*, 101(9), 2304–2313.

Oguntola, M. B., Kinyanjui, M. N., & Ogonji, J. A. (2018). Effects of structural viscoelasticity in non-divergence free deformable porous media with incompressible constituents. *Global Journal of Pure and Applied Mathematics*, *14*(8), 1121–1147.

O'Neil, P. V. (2011). *Beginning partial differential equations*, volume 85. John Wiley & Sons.

Osidak, M., Osidak, E., Akhmanova, M., Domogatsky, S., & Domogatskaya, A. (2015). Fibrillar, fibril-associated and basement membrane collagens of the arterial wall: architecture, elasticity and remodeling under stress. *Current pharmaceutical design*, *21*(9), 1124–1133.

Ovchinnikov, S. (2018). *Functional Analysis: An Introductory Course*. Universitext. Springer International Publishing.

Owczarek, S. (2010). A galerkin method for biot consolidation model. *Mathematics and Mechanics of Solids*, *15*(1), 42–56.

Paola, C., Guidoboni, G., Harris, A., Prada, D., Sacco, R., & Terragni, S. (2014). A poroelastic model for the perfusion of the lamina cribrosa in the optic nerve head. *Mathematical biosciences*, 257, 33–41.

Recha-Sancho, L., Moutos, F. T., Abellà, J., Guilak, F., & Semino, C. E. (2016). Dedifferentiated human articular chondrocytes redifferentiate to a cartilage-like tissue phenotype in a poly (epsilon-caprolactone) self-assembling peptide composite scaffold. *Materials*, 9(6), 472.

Rendulic, L. (1936). Porenziffer und porenwasserdruck in tonen (void ratio and pore pressure in clays). *Der Bauingenieur*, *17*, 559–564.

Sack, I., Beierbach, B., Wuerfel, J., Klatt, D., Hamhaber, U., Papazoglou, S., Martus, P., & Braun, J. (2009). The impact of aging and gender on brain viscoelasticity. *Neuroimage*, *46*(3), 652–657.

Selvadurai, A. P. S. (2003). On the mechanics of damage-susceptible poroelastic media. *In Key Engineering Materials. Trans Tech Publications.*, (Vol. 251, pp. 363–374).

Serpieri, R. & Travascio, F. (2017). *Variational Continuum Multiphase Poroelasticity*. Springer.

Shabana, A. A. (2018). *Computational Continuum Mechanics* (3rd ed.). Wiley.

Showalter, R. E. (2000). Diffusion in poro-elastic media. *Journal of mathematical analysis and applications*, *251*(1), 310–340.

Siddique, J. I., Ahmed, A., Aziz, A., & Khalique, C. M. (2017). Theory for deformable porous media and applications. *Applied Sciences,*, 7(9), 917.

Simon, B. R., Wu, J. S., Carlton, M. W., Kazarian, L. E., France, E. P., Evans, J. H., & Zienkiewicz, O. C. (1985). Volvo award in biomechanics: Poroelastic dynamic structural models of rhesus spinal motion segments. *Spine*, 10(6), 494–507.

Soltz, M. A. & Ateshian, G. A. (1998). Experimental verification and theoretical prediction of cartilage interstitial fluid pressurization at an impermeable contact interface in confined compression. *Journal of biomechanics*, *31*(10), 927–934.

Tirella, A., Mattei, G., & Ahluwalia, A. (2014). Strain rate viscoelastic analysis of soft and highly hydrated biomaterials. *Journal of Biomedical Materials Research Part A,*, 102(10), 3352–3360.

Verri, M., Guidoboni, G., Bociu, L., & Sacco, R. (2017). The role of structural viscoelasticity in deformable porous media with incompressible constituents: applications in biomechanics. *American Institute for Mathematical Science*.

von Terzaghi, C. (1925). *Erdbaumechanik auf bodenphysikalischer Grundlage*. Deuticke.

Von Terzaghi, K. (1923). Die berechnung der durchassigkeitsziffer des tones aus dem verlauf der hydrodynamischen spannungs. erscheinungen. *Sitzungsber. Akad. Wiss. Math. Naturwiss. Kl. Abt. 2A*, *132*, 105–124.

Wang, H. F. (2017). *Theory of linear poroelasticity with applications to geomechanics and hydrogeology*. Princeton University Press.

Yang, Z. (2006). *Poroviscoelastic dynamic finite element model of biological tissue*. PhD thesis, University of Pittsburgh.

Yuan, Z. (2014). Model-based quantification of blood flow rate and oxygen consumption rate of biological tissues using image-guided near infrared light spectroscopy.

APPENDIX A

MATLAB SCRIPTS

A.1 Dimensionless solid displacement $\hat{u}_{\hat{\beta}}(\hat{x},\hat{t})$

```
% this script computes the dimensionless displacement
% as a function of x and t, for a given value of beta, in
% the case where F(t) = step pulse
close all
clear all
%
xmin = 0;
xmax = 1;
xst  = 25;
dx   = (xmax-xmin)/xst;
tmin = 0;
tmax = 3;
tst  = 25;
dt   = (tmax-tmin)/tst;
xx   = xmin:dx:xmax;
tt   = [tmin:dt:tmax];
beta  = 0;
tol  = eps;
nmax = 100000;
%
for i = 1:numel(xx),
```

```
x = xx(i);
for j = 1:numel(tt);
t = tt(j);
n = 1;
absterm = tol + 1;
U(i,j)  = -x;
while ((n <= nmax) & (absterm > tol))
ln = (2*n-1)^2*pi^2/4;
yn = sin((2*n-1)/2*pi*x);
term = (-1)^(n-1)/ln*exp(-ln*t/(1+beta*ln))*yn;
%absterm = abs(term);
U(i,j)  = (U(i,j) + 2*term);
n       = n+1;
end
end
end
U_beta_0 = U;
%
xmin = 0;
xmax = 1;
xst  = 25;
dx   = (xmax-xmin)/xst;
tmin = 0;
tmax = 3;
tst  = 25;
dt   = (tmax-tmin)/tst;
%
xx   = [xmin:dx:xmax];
tt   = [tmin:dt:tmax];
%
```

```
beta  = 1;
tol   = eps;
nmax = 100000;
%
for i = 1:numel(xx),
x = xx(i);
for j = 1:numel(tt)
t = tt(j);
n = 1;
absterm = tol + 1;
U(i,j)  = -x;
while ((n <= nmax) & (absterm > tol))
ln = (2*n-1)^2*pi^2/4;
 yn = sin((2*n-1)/2*pi*x);
 term = (-1)^(n-1)/ln*exp(-ln*t/(1+beta*ln))*yn;
 %absterm = abs(term);
 U(i,j)  = (U(i,j) + 2*term);
 n       = n+1;
end
end
end
%
U_beta_1 = U;
%
setfonts
%
figure
subplot(1,2,1);
surf(xx,tt,U_beta_0')
axis square
```

A.2 Dimensionless discharge velocity $\hat{v}_{\hat{\beta}}(\hat{x}, \hat{t})$

```
% this script computes the dimensionless velocity
% as a function of x and t, for a given value of beta, in
% the case where F(t) = step pulse
close all
Nt = 20;
Nx = 20;
L  = 1;
beta = 0;
t  = 0:3/(Nt-1):3;
x  = 0:L/(Nx-1):L;
[t,x] = meshgrid(t,x);
q = zeros(Nx,Nt);
M = 22200;
for n = 1:M
    an = (2*n-1)/(2*L);
    bn = an*pi;
    cn = bn^2;
    An = (-1)^(n-1)/(1+beta*cn);
    xn = exp(-cn*t/(1+beta*cn));
    yn = sin(an*pi*x);
    q = (q + 2.*An.*yn'.*xn');
end
V_beta_0 = log10(abs(q));
%
Nt = 20;
Nx = 20;
L  = 1;
```

```
beta=1;
t  = 0:3/(Nt-1):3;
x  = 0:L/(Nx-1):L;
[t,x] = meshgrid(t,x);
p = zeros(Nx,Nt);
M = 22000;
et=1;
p=zeros(Nx,Nt);
for n = 1:M
    an = (2*n-1)/(2*L);
    bn = an*pi;
    cn = bn^2;
    An = (-1)^(n-1)/(1+beta*cn);
    xn = exp(-cn*t/(1+beta*cn));
    yn = sin(an*pi*x);
    p = (p + 2*An.*yn'.*xn');
end
V_beta_1 = log10(abs(p));
```

A.3 Dimensionless fluid power density $\hat{\mathcal{P}}_{\hat{\beta}}(\hat{t})$

```
% this script computes the dimensionless power density
% as a function of t, for a given value of beta, in
% the case where F(t) = step pulse
clear all
close all
Nt = 200;
L = 1;
beta = 0.1;
t  = 0:3/(Nt-1):3;
```

```
q = 0;
M = 100000;
for n= 1:M
      an = (2*n-1)/(2*L);
      bn = an*pi;
      cn = bn^2;
      An = 2/(1+beta*cn)^2;
      xn = exp(-2*cn*t/(1+beta*cn));
      q = (q + An.*xn);
end
P_beta_0 = log10(q);
Nt = 200;
L = 1;
beta=1;
t  = 0:3/(Nt-1):3;
q = 0;
M = 10000;
for n= 1:M
      an = (2*n-1)/(2*L);
      bn = an*pi;
      cn = bn^2;
      An = 2/(1+beta*cn)^2;
      xn = exp(-2*cn*t/(1+beta*cn));
      q = (q + An.*xn);
end
P_beta_1 = log10(q);
```

A.4 Dimensionless Velocity $\hat{v}_{\hat{\beta}}(\hat{x}, 0)$ for $\hat{\beta} \in [0, 1]$

```
% this script computes the dimensionless velocity
```

```
% at t=0, for a given value of beta, in
% the case where F(t) = step pulse
clear all
close all
Nx = 28;
L = 1;
beta = 0;
x  = 0:L/(Nx-1):L;
q = 0;
M = 890000;
for n= 1:M
      an = (2*n-1)/(2*L);
      bn = an*pi;
      cn = bn^2;
      An = (-1)^(n-1)/(1+beta*cn);
      yn = sin(an*pi*x);
      q = (q + 2*An.*yn);
end
V_beta_0 = log10(abs(q));

L = 1;
beta = 0.2;
x  = 0:L/(Nx-1):L;
q = 0;
for n= 1:M
      an = (2*n-1)/(2*L);
      bn = an*pi;
      cn = bn^2;
      An = (-1)^(n-1)/(1+beta*cn);
      yn = sin(an*pi*x);
```

```
        q = (q + 2*An.*yn);
end
V_beta_6 = log10(abs(q));
L = 1;
beta = 0.4;
x  = 0:L/(Nx-1):L;
q = 0;
for n= 1:M
        an = (2*n-1)/(2*L);
        bn = an*pi;
        cn = bn^2;
        An = (-1)^(n-1)/(1+beta*cn);
        yn = sin(an*pi*x);
        q = (q + 2*An.*yn);
end
V_beta_7 = log10(abs(q));

%Nx = 30;
L = 1;
beta = 0.5;
x  = 0:L/(Nx-1):L;
q = 0;
%M = 890000;
for n= 1:M
        an = (2*n-1)/(2*L);
        bn = an*pi;
        cn = bn^2;
        An = (-1)^(n-1)/(1+beta*cn);
        yn = sin(an*pi*x);
        q = (q + 2*An.*yn);
```

```
end
P_beta_5 = log10(abs(q));


L = 1;
beta = 1;
x  = 0:L/(Nx-1):L;
q = 0;
%M = 890000;
for n= 1:M
      an = (2*n-1)/(2*L);
      bn = an*pi;
      cn = bn^2;
      An = (-1)^(n-1)/(1+beta*cn);
      yn = sin(an*pi*x);
      q = (q + 2*An.*yn);
end
P_beta_1 = log10(abs(q));
```

A.5 Dimensionless maximum discharge Velocity $\hat{v}_{\hat{\beta}}(\hat{\beta})$ and dimensionless power density $\hat{\mathcal{P}}_{\hat{\beta}}(\hat{\beta})$

```
% this script computes the dimensionless maximum velocity
% and dimensionless power density as a function of beta
% in the case where F(t) = step pulse
clear all
close all
Nx = 200;
L = 1;
beta  = 0:L/(Nx-1):L;
q = 0;
```

```
M = 30000;
for n= 1:M
      an = (2*n-1)/(2*L);
      bn = an*pi;
      cn = bn^2;
      q = (q + 2*(1./(1+beta*cn)));
end
V_max = log10(q);
Nx = 200;
L = 1;
a = 1
beta  = 0:L/(Nx-1):L;
q = 0;
M = 30000;
for n= 1:M
      an = (2*n-1)/(2*L);
      bn = an*pi;
      cn = bn^2;
      q = (q + 2*(1./(1+beta*cn).^2))*1/a;
end
P_max = log10(q);
```

A.6 Dimensionless maximum discharge Velocity $\hat{v}_{\hat{\beta}}(\hat{\beta})$ and dimensionless power density $\hat{\mathcal{P}}_{\hat{\beta}}(\hat{\beta})$ for $F_{spec} \in [10^{-4}, 10^{4}]$

```
% this script computes the dimensionless maximum velocity
% and dimensionless power density as a function of beta
%for a given value of the magnitude of F(t), in
% the case where F(t) = step pulse
clear all
```

```
close all
Nx = 200;
L = 1;
beta  = 0:L/(Nx-1):L;
Pr = 10^(-2);
q = 0;
M = 100000;
for n= 1:M
      an = (2*n-1)/(2*L);
      bn = an*pi;
      cn = bn^2;
      q = (q + 2.*Pr.*(1./(1+beta*cn)));
end
V_max = log10(q);
%plot(t,P_eta_0)

Pr=10^(-1);
for n= 1:M
      an = (2*n-1)/(2*L);
      bn = an*pi;
      cn = bn^2;
      q = (q + 2.*Pr.*(1./(1+beta*cn)))*1/a;
end
V_max1 = log10(q);

Pr=1;
for n= 1:M
      an = (2*n-1)/(2*L);
      bn = an*pi;
      cn = bn^2;
```

```
      q = (q + 2.*Pr.*(1./(1+beta*cn)))*1/a;
end
V_max2 = log10(q);

Pr=10;
for n= 1:M
      an = (2*n-1)/(2*L);
      bn = an*pi;
      cn = bn^2;
      q = (q + 2.*Pr.*(1./(1+beta*cn)))*1/a;
end
V_max3 = log10(q);

Pr=10^2;
for n= 1:M
      an = (2*n-1)/(2*L);
      bn = an*pi;
      cn = bn^2;
      q = (q + 2.*Pr.*(1./(1+beta*cn)))*1/a;
end
V_max4 = log10(q);

Pr=10^3
for n= 1:M
      an = (2*n-1)/(2*L);
      bn = an*pi;
      cn = bn^2;
      q = (q + 2.*Pr.*(1./(1+beta*cn)))*1/a;
end
V_max5 = log10(q);
```

```
Pr=10^(4)
for n= 1:M
      an = (2*n-1)/(2*L);
      bn = an*pi;
      cn = bn^2;
      q = (q + 2.*Pr.*(1./(1+beta*cn)))*1/a;
end
V_max6 = log10(q);
%

Nx = 200;
L = 1;
Pr = 10^(-2);
a = 1
beta  = 0:L/(Nx-1):L;
q = 0;
M = 100000;
for n= 1:M
      an = (2*n-1)/(2*L);
      bn = an*pi;
      cn = bn^2;
      q = (q + 2.*Pr .*(1./(1+beta*cn).^2))*1/a;
end
P_max = log10(q);

Pr=10^(-1);
for n= 1:M
      an = (2*n-1)/(2*L);
      bn = an*pi;
```

```
    cn = bn^2;
    q = (q + 2.*Pr.*(1./(1+beta*cn).^2))*1/a;
end
P_max1 = log10(q);

Pr = 1

for n= 1:M
    an = (2*n-1)/(2*L);
    bn = an*pi;
    cn = bn^2;
    q = (q + 2.*Pr.*(1./(1+beta*cn).^2))*1/a;
end
P_max2 = log10(q)

Pr=10;
for n= 1:M
    an = (2*n-1)/(2*L);
    bn = an*pi;
    cn = bn^2;
    q = (q + 2.*Pr.*(1./(1+beta*cn).^2))*1/a;
end
P_max3 = log10(q);

Pr=10^(2);
for n= 1:M
    an = (2*n-1)/(2*L);
    bn = an*pi;
    cn = bn^2;
    q = (q + 2.*Pr.*(1./(1+beta*cn).^2))*1/a;
```

```
end
P_max4 = log10(q);

Pr=10^(3);
for n= 1:M
      an = (2*n-1)/(2*L);
      bn = an*pi;
      cn = bn^2;
      q = (q + 2.*Pr.*(1./(1+beta*cn).^2))*1/a;
end
P_max5 = log10(q);

Pr=10^(4);
for n= 1:M
      an = (2*n-1)/(2*L);
      bn = an*pi;
      cn = bn^2;
      q = (q + 2.*Pr.*(1./(1+beta*cn).^2))*1/a;
end
P_max6 = log10(q);
```

A.7 Dimensionless discharge velocity $\hat{v}^*_{\hat{\beta}}(\hat{x}, \hat{t})$

```
% this script computes the dimensionless discharge velocity
% as a function of x and t, for a given value of beta, xi, a and tau,
% in the case where F(t) = trapezoidal pulse
close all
clear all
a=1
xmin = 0;
```

```
xmax = 1;
xst  = 30;
dx   = (xmax-xmin)/xst;
tmin = 0;
tmax = 2;
tst  = 40;
dt   = (tmax-tmin)/tst;
xx   = [xmin:dx:xmax];
tt   = [tmin:dt:tmax];
beta  = 0.012;
tol  = eps;
nmax = 100000;
xi = 0.21;
tau     = 1;
for i = 1:numel(xx),
x = xx(i);
for j = 1:numel(tt)
t = tt(j);
V(i,j) = a/xi*(-U_step(x,t,beta)*Heaviside(t) + ...
U_step(x,t-xi,beta)*Heaviside(t-xi) + ...
U_step(x,t-tau-xi,beta)*Heaviside(t-tau-xi) - ...
U_step(x,t-tau-2*xi,beta)*Heaviside(t-tau-2*xi));
end
end
```

A.7.1 The Unit-step function for $\hat{v}^*_{\hat{\beta}}(\hat{x},\hat{t})$

```
% this script computes the Unit-step function (F(t))
function F = U_step(xx,tt,eta)
tol  = eps;
nmax = 100000;
```

```
for i = 1:numel(xx),
x = xx(i);
for j = 1:numel(tt)
t = tt(j);
n = 1;
absterm = tol + 1;
U(i,j)  = -x;
while ((n <= nmax) & (absterm > tol))
ln = (2*n-1)^2*pi^2/4;
yn = sin((2*n-1)/2*pi*x);
term = (-1)^(n-1)/ln*exp(-ln*t/(1+beta*ln))*yn;
absterm = term;
U(i,j)  = (U(i,j) + 2*term);
n       = n+1;
end
end
end
F = U;
end
```

A.8 Dimensionless fluid power density $\hat{\mathcal{P}}^*_{\hat{\beta}}(\hat{t})$

```
% this script computes the dimensionless power density
% as a function of t, for a given value of beta, xi and tau,
% in the case where F(t) = trapezoidal pulse
close all
clear all
syms x
a=1;
tmin = 0;
```

```
tmax = 2;
tst  = 100;
dt   = (tmax-tmin)/tst;
tt   = [tmin:dt:tmax];
beta  = 0.012;
tol  = eps;
epsilon = 0.21;
tau     = 1;
for j = 1:numel(tt)
t=tt(j);
P(j) = (a/epsilon)^2*int((U_eta(x,t,beta)*Heaviside(t) - ...
U_beta(x,t-epsilon,beta)*Heaviside(t-epsilon) - ...
U_beta(x,t-tau-epsilon,beta)*Heaviside(t-tau-epsilon) + ...
U_beta(x,t-tau-2*epsilon,beta)*Heaviside(t-tau-2*epsilon))^2,x,0,1);
end
```

A.8.1 The U_β function for $\hat{\mathcal{P}}^*_{\hat{\beta}}(\hat{t})$

```
function U = U_beta(x,t,beta)
syms x
L  = 1;
q = 0;
nmax = 10;
for n = 1:nmax
    an = (2*n-1)/(2*L);
    bn = an*pi;
    cn = bn^2;
    An = -2 *(-1)^n./cn;
    xn = exp(-cn*t/(1+beta*cn));
    yn = sin(an*pi*x);
    q = (q + An.*(1-xn).*yn);
```

```
end
U=q;
end
```

A.9 Dimensionless maximum discharge velocity $\hat{v}^*_{\max}(\hat{\beta}, \hat{\xi})$

```
% this script computes the dimensionless maximum velocity
% as a function of beta and xi
% in the case where F(t) = trapezoidal pulse
Nx = 30;
Nt = 30;
L = 1;
beta = linspace(0,0.01,Nx) ;
epsi = linspace(0,0.01,Nt) ;
[Beta,Xi] = meshgrid(beta,epsi);
q = zeros(Nx,Nt);
M = 10000;
for n= 1:M
      an = (2*n-1)/(2*L);
      bn = (an*pi)^2;
      An=1./bn;
      Xn=exp(-bn.*Xi./(1+Beta.*bn));
      cn = 1-Xn;
      q = (q + An.*cn);
end
setfonts
V_max = (2./Xi).*q;
```

A.10 Matlab Code for Figure 4.2

```
clear all
```

```
close all
Nx = 60;
Nt = 60;
L = 0.81*10^(-3);
beta = linspace(0,0.01,Nx) ;
xi = linspace(0,0.01,Nt) ;
[Beta,Xi] = meshgrid(xi,beta);
q = zeros(Nx,Nt);
M = 20000;
for n= 1:M
      an = (2*n-1)/(2*L);
      bn = an*pi;
      An=1./bn;
      Xn=exp(-bn.*Xi./(1+Beta.*bn));
      cn = 1-Xn;
      q = (q + An.*cn);
end
V_max = 12+(2./Xi).*q;
t=ones(Nx,Nt);
for n= 1:M
V=16.3*t;
end
```

A.11 Matlab Code for Figure 4.3

```
clear all
close all
m = 120; n = 120;
beta = linspace(0.00001,0.01,m) ;
xi = linspace(0.00001,0.01,n) ;
```

```
[X,Y] = meshgrid(beta,xi) ;
L = 1;
N = 20;
Q = zeros(m,n) ;
for i = 1:N
    vn = ((2*i-1)/2*L)^2*pi^2 ;
    A = -vn*X./(1+vn*Y) ;
    Q = Q+1/vn*(1-exp(A))  ;
end
t=ones(m,n);
for i=1:N
C=16.3*t;
end
Q = 2./X.*Q ;
```